Geoscience Frontiers 10 (2019) 2313–2327

Contents lists available at ScienceDirect

China University of Geosciences (Beijing)

Geoscience Frontiers

journal homepage: www.elsevier.com/locate/gsf

Research Paper

The northern Qiangtang Block rapid drift during the Triassic Period: Paleomagnetic evidence

Yanan Zhou [a], Xin Cheng [a], Yiying Wu [a], Vadim Kravchinsky [b], Ruiqi Shao [a], Weijie Zhang [a], Bitian Wei [a], Ruiyao Zhang [a], Fanrong Lu [a], Hanning Wu [a,*]

[a] Department of Geology & State Key Laboratory of Continental Dynamics, Northwest University, Xi'an 710069, China
[b] Department of Physics, University of Alberta, AB, Canada

ARTICLE INFO

Article history:
Received 15 July 2018
Received in revised form
28 March 2019
Accepted 6 May 2019
Available online 21 May 2019
Handling Editor: Wenjiao Xiao

Keywords:
Northern Qiangtang block
Paleomagnetism
Plate tectonics
Tethys ocean
Tibetan plateau
Triassic

ABSTRACT

As one of the pivotal Gondwana–derived blocks, the kinematic history of the northern Qiangtang Block (in the Tibetan Plateau) remains unclear, mainly because quantitative paleomagnetic data to determine the paleoposition are sparse. Thus, for this study, we collected 226 samples (17 sites) from Triassic sedimentary rocks in the Raggyorcaka and Tuotuohe areas of the northern Qiangtang Block (NQB). Stepwise demagnetization isolated high temperature/field components from the samples. Both Early and Late Triassic datasets passed field tests at a 99% confidence level and were proved to be primary origins. Paleopoles were calculated to be at 24.9°N and 216.5°E with $A_{95} = 8.2°(N = 8)$ for the Early Triassic dataset, and at 68.1°N, 179.9°E with $A_{95} = 5.6°$ ($N = 37$) for the Late Triassic, the latter being combined with a coeval volcanic dataset published previously. These paleopoles correspond to paleolatitudes of 14.3°S±8.2° and 29.9°N±5.6°, respectively. Combining previously published results, we reconstructed a three-stage northward drift process for the NQB. (1) The northern Qiangtang Block was located in the subtropical part of the southern hemisphere until the Early Triassic; (2) thereafter, the block rapidly drifted northward from southern to northern hemispheres during the Triassic; and (3) the block converged with the Eurasian continent in the Late Triassic. The ~4800 km northward movement from the Early to Late Triassic corresponded to an average motion rate of ~11.85 cm/yr. The rapid drift of the NQB after the Early Triassic led to a rapid transformation of the Tethys Ocean.

1. Introduction

The Tibetan Plateau was formed from the split and drift of microcontinent; multi-stage subductions; continental-continental collisions; and the intracontinental convergence that accompanied the expansion and closure of multiple Tethyan ocean basins (e.g. Chang and Zheng, 1973; Allégre et al., 1984; Huang and Chen, 1987; Dewey et al., 1988; Zhong and Ding, 1996; Yin and Harrison, 2000; Ren and Xiao, 2004; Wang et al., 2010; Pan et al., 2012; Xiao et al., 2015, 2017; Zhu et al., 2016; Ding et al., 2017). The collision and ceaseless northward indentation of India into Eurasia resulted in the ultimate uplift of the Tibetan Plateau, the most distinct elevated region on the Earth (e.g. Tapponnier et al., 2001; Calais et al., 2003; Aitchison et al., 2007; Wu et al., 2008; Dupont–Nivet et al., 2010). More and more geological and geophysical evidence has revealed that the Tibetan Plateau was formed by successive rifting and northward drifting of Gondwana–derived microcontinents that subsequently accreted onto the southern margin of Eurasia (e.g. Huang et al., 2010; Liebke et al., 2010; Yang et al., 2015; Yan et al., 2016; Yi et al., 2016; Li et al., 2017; Sun et al., 2019). The proto–plateau had already taken shape before the final collision between India and Eurasia (Lippert et al., 2010; Dai et al., 2012). A thorough understanding of the complex formation of the Tibetan Plateau requires a restoration of the kinematic history of the Gondwana-derived blocks before the collision between India and Eurasia.

As one of the key points for understanding the growth process of the plateau, the kinematic history of northern Qiangtang Block (NQB) remains unclear. Qualitative constraints on the movement of NQB rely on geological evidence such as the interpretation of stratigraphic sequences, a review of paleontological assemblages,

* Corresponding author.
E-mail address: wuhn2506@nwu.edu.cn (H. Wu).
Peer-review under responsibility of China University of Geosciences (Beijing).

https://doi.org/10.1016/j.gsf.2019.05.003

and the timing of tectono-thermal events. The presence of the Pan–African basement (Wang and Wang, 2001; Zheng et al., 2015; Li et al., 2016a) suggests that the NQB was of Gondwanan origin. The glacial-marine deposits associated with cold-water biota from the Permian Period (Wang, 1984; Metcalfe, 1996; Pullen and Kapp, 2014), as well as collision markers from the Late Triassic, were preserved and discovered in the NQB (Ding et al., 2013; Dan et al., 2018). Some authors have therefore suggested that it drifted after the Permian and amalgamated with Eurasia in the Late Triassic (Ding et al., 2017; Song et al., 2017). However, other geochemical data and phytogeographical evidence indicate that the NQB drifted northward and accreted onto Eurasian between the Carboniferous and Permian (Pearce and Mei, 1988; Bian et al., 1997; Golonka and Ford, 2000; Liu and Sun, 2008). A primary reason for this controversy is that the drift history of the NQB has not yet been clearly interpreted.

When the paleolongitude is indeterminate, paleomagnetism is the only quantitative method to reconstruct the kinematic evolution of continental blocks (Huang et al., 2018). Previously published paleomagnetic data, even data derived from different lithological units, indicated a similar drift trend, which suggested that the NQB was located in the subtropical southern hemisphere prior to the Late Permian (Cheng et al., 2012a, 2013; Song et al., 2017; Yang et al., 2017; Zhang, 2017; Ma et al., 2019), and ultimately merged into the mainland of Eurasia in the Late Triassic (e.g. Otofuji et al., 1990; Huang et al., 1992a,b; Chen et al., 1993; Cheng et al., 2012b; Tong et al., 2015; Yan et al., 2016; Chen et al., 2017; Ran et al., 2017; Cao et al., 2019). Previous datasets, therefore, suggest that the Triassic was the crucial period for the northward movement of the NQB, but could not ascertain more movement details for the critical period. Only rough constraints were indicated by the sparse paleomagnetic data to quantify the Late Triassic paleo-position (Ye and Li, 1987; Lin and Watts, 1988; Song et al., 2012, 2015), especially, there is a lack of reliable paleomagnetic data reported for the Early and Middle Triassic.

To add more data to previous datasets, in this study, we present two paleomagnetic datasets for Early Triassic and Late Triassic periods, and estimate the latitudinal displacement and velocities of the northern Qiangtang Block during the Triassic Period. Based on these results and published data, we define a three-stage northward drift history of the NQB, and reconstruct the Triassic paleogeography of this block and adjacent terrain.

2. Geological setting and paleomagnetic sampling

The NQB is separated from the Songpan–Ganzi Block to the north by the Xijin Ulan-Jinshajiang Suture (XJS), and from the southern Qiangtang Block to the south by the Longmu

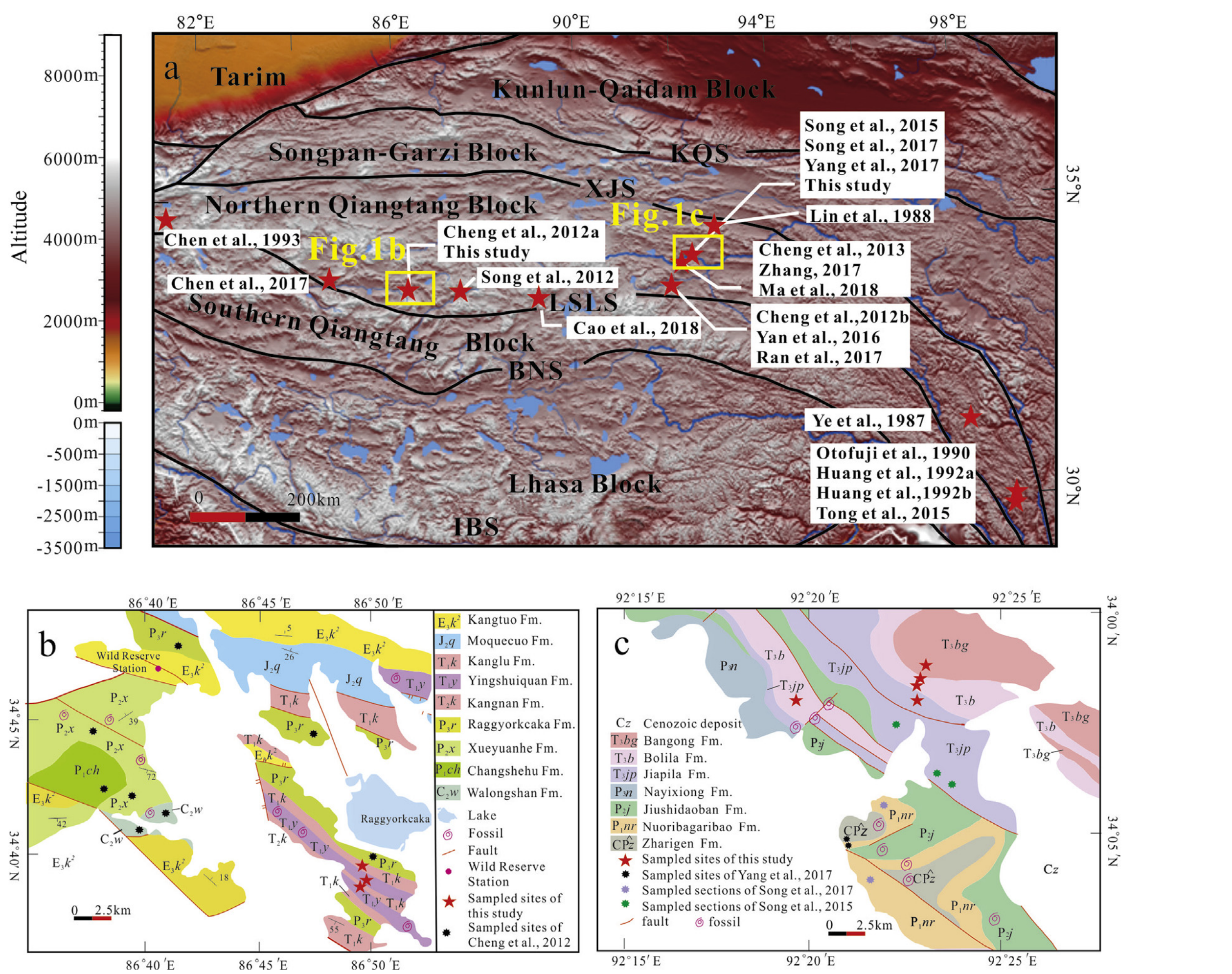

Fig. 1. Geological structure map showing the major blocks and sutures on the Tibetan Plateau, and the locations of previous paleomagnetic studies conducted in the NQB (red five-point stars) (a). Geologic maps of the Early Triassic (b) and Late Triassic (c) sampling areas showing the distributions of paleomagnetic site locations. Abbreviations: IBS–Indus-Yarlung Zangbo suture zone; BNS–Bangong-Nujiang suture zone; LSLS–Lungmu Co-Shuanghu suture zone; XJS–Xijin Ulan-Jinshajiang suture zone; KQS–Kunlun-Qinlin suture zone. Yellow box: study area.

Co–Shuanghu suture (LSLS) (Fig. 1a) (e.g., Zhang et al., 2006; Li et al., 2009; Zhang et al., 2013). The NQB is a large, stable block with a Precambrian crystalline basement and Phanerozoic sedimentary cover in which continuous Upper Devonian to Lower Triassic sedimentary sequences are overlain by the Middle–Lower Jurassic and Cenozoic rocks (BGMR, 1993; Li and Zheng, 1993; Qinghai BGMR, 2005). For the Triassic rocks, the Upper Triassic strata are exposed only in the Raggyorcaka area, whereas the Lower Triassic strata are easier found throughout this block. Based on field investigations, we chose the Raggyorcaka and Tuotuohe areas, where these strata are well exposed and preserved for sampling.

2.1. Geology of the Lower Triassic rocks

In the Raggyorcaka area (Fig. 1b), the sedimentary succession was continuously deposited from the Late Carboniferous to the Middle Triassic, and the sediments were successive stable shallow marine deposits (BGMR, 1993). The Lower Triassic strata, including the Yingshuiquan and Kanglu formations, are well preserved in this area.

The Yingshuiquan Formation (Fig. 2a), which conformably underlies the Kangnan Formation, is dominated by calcareous sandstone and gray or gray-green limestone (Zhu et al., 2005, 2010). Abundant conodont fossils, such as *Hibbardelloides* sp., *Pachyclaina oblique*, and *Pachycladina* sp., have been found in the Yingshuiquan Formation. Analysis of the conodont biofacies suggests a formation of Olenekian age in the Early Triassic. The estimation is supported by detrital zircon LA–ICP–MS data from the Yingshuiquan Formation that present a maximum depositional age of 249 Ma (Xie et al., 2018). The Kanglu Formation (T_1k) was continuously deposited in the Upper Permian Raggyorcaka Group, and conformably underlies the Lower Triassic Yingshuiquan Formation (T_1y) (Guo, 2013; Qu et al., 2015). The Kanglu Formation comprises, from bottom to top, siltstone, silty mudstone, sandstone, and limestone. Bivalve fossils, especially *Claraia aurita*, *C. aurita haueri*, and *C. stachei*, are abundantly preserved in this formation, and indicate an age in the early stage of the Early Triassic.

The Yingshuiquan and Kanglu formations are symmetrically distributed along the two limbs of the Raggyorcaka anticline. The Upper Permian Raggyorcaka Formation comprises the nucleus of this fold. Late Triassic intrusive rock were not involved into the Raggyorcaka anticline, which indicates that the main deformation phase proceeded prior to the Late Triassic (Lei et al., 2001; Li et al., 2008).

2.2. Geology of the Upper Triassic Jiezha Group

In the Tuotuohe area (Fig. 1c), the Upper Triassic Jiezha Group is characterized by continual shallow marine deposits in which biota flourished (Qinghai BGMR, 2005). The Jiezha Group refers to a set of clastic and carbonate sediments that overlie the Upper Permian strata with an angular unconformity. This group, from bottom to top, includes the Jiapila, Bolila, and Bagong formations. Lithologically, the Jiapila Formation consists mainly of clastic rocks bearing andesite and limestone (Fig. 2b). The Bolila Formation is composed of gray micrite, calcite dolomite which interbed with sandstone. The Bagong Formation primarily consists of quartz sandstone and carbonaceous shale interbedded with limestone lenses, bears coal seams (streaks) (Fig. 2c). These three formations conform with one another sequentially. The paleontological assemblage, such as *Quemocuomegalodon orientus-Neomegalodon cornutus* from the Jiapila Formation, *H. superbescens*, *H. disperseinsecta* from the Bolila and Bagong formations, are recognized in these strata, and indicate a Norian age (Late Triassic) (Tang et al., 2011).

The Jiezha Group is unconformably overlain by the Middle–Upper Jurassic Yanshiping Group in the sampling area (e.g., Li et al., 2012). Besides, the deformations in strata had occurred in the Middle–Upper Jurassic and the Upper Triassic are entirely different. Therefore, we propose that the folding of the Jiezha Group

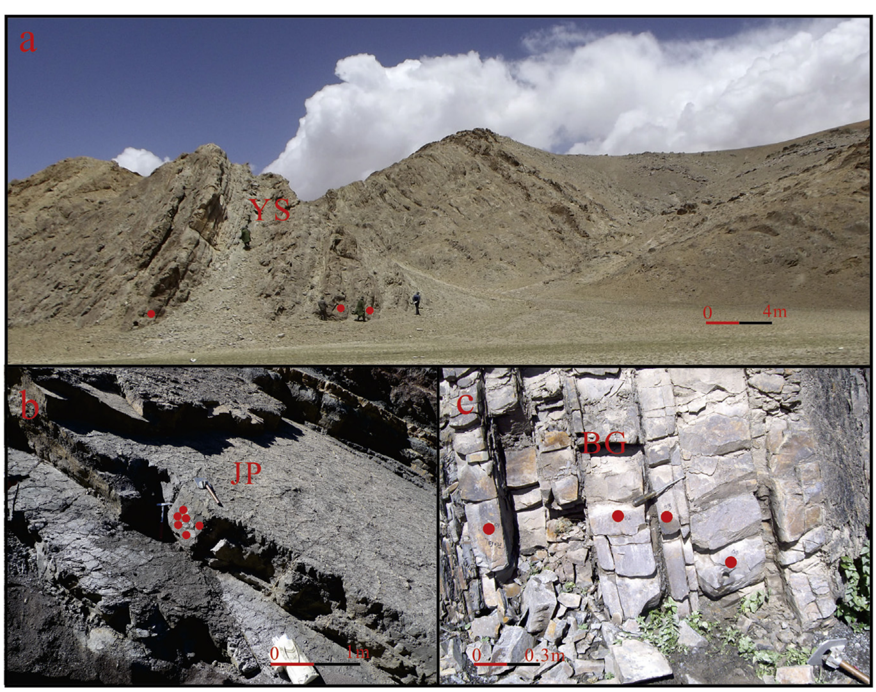

Fig. 2. Photos showing the Lower and Upper Triassic sedimentary sequences of sampled strata. The sampled section of the Yingshuiquan Formation (a), representative photos of sampled rocks (b and c). Abbreviations: YS–Yingshuiquan Formation; JP–Jiapeila Formation; BG–Bagong Formation.

occurred in the Late Triassic–Early Jurassic (Li et al., 2008; Song et al., 2015).

2.3. Sampling

We drilled 226 samples from 17 sites using portable petrol-powered drilling. Eight sites (112 samples) were in the Lower Triassic Yingshuiquan and Kanglu formations (sites ID, YS, and KL) near Raggyorcaka Lake (33.7°N, 86.9°E), and nine sites (114 samples) were in the Upper Triassic Jiezha Group (sites ID, BG, BL, and JP) along the Qinghai–Tibet highway in the Tuotuohe area (92.4°E, 34.1°N). Paleomagnetic samples were oriented using both Sun and magnetic compasses. All oriented cores, 2.54 cm in diameter, were cut into standard specimens (2.2-cm-long) in the laboratory for further research.

3. Laboratory procedures

Rock magnetic measurements and demagnetization experiments were carried out in a shielded magnetic space with a residual field of less than 300 nT, in the Paleomagnetism and Chronology Laboratory at the Institute of Geology and Geophysics, Chinese Academy of Sciences, and the Magnetotectonics Laboratory at Peking University, Beijing, China. To choose the demagnetization

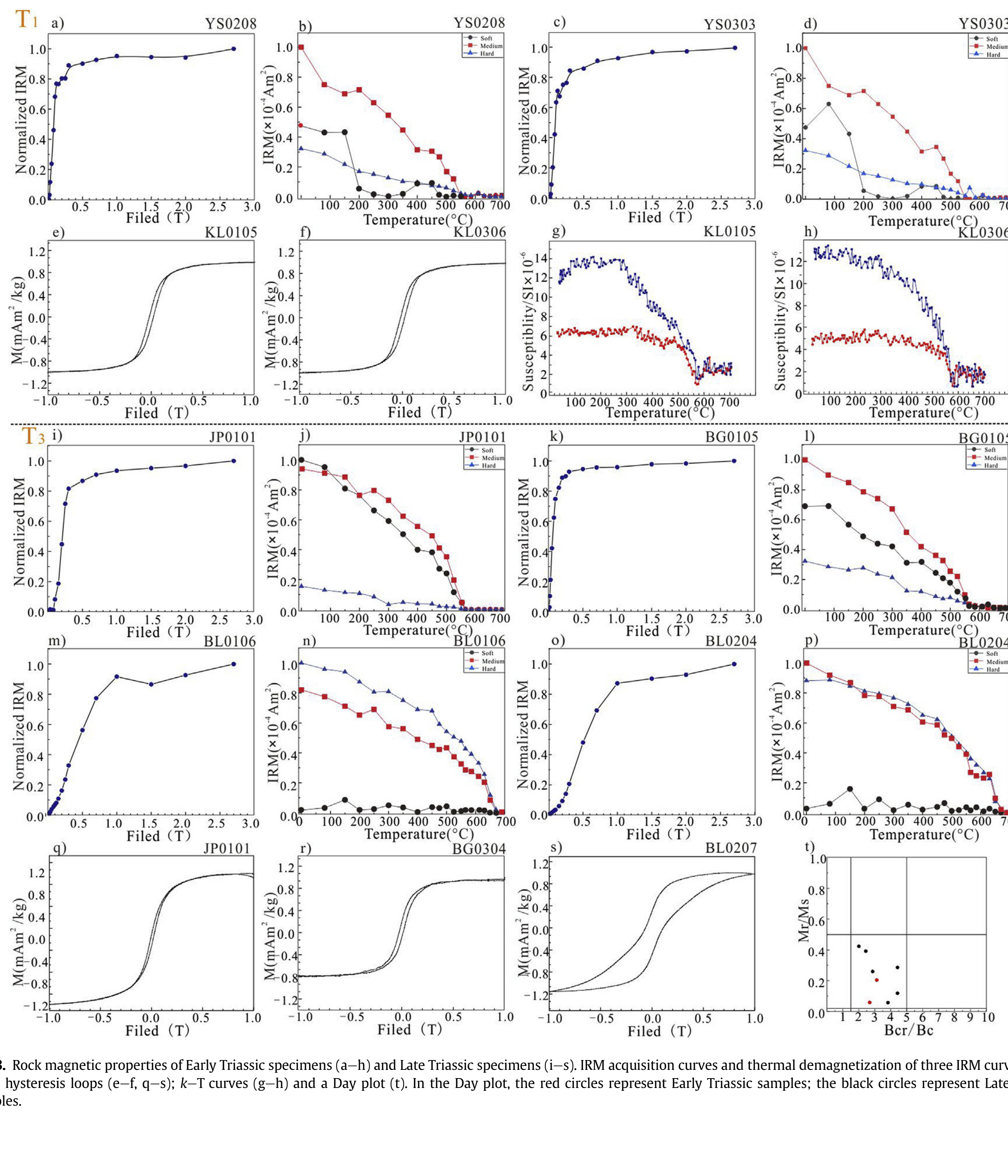

Fig. 3. Rock magnetic properties of Early Triassic specimens (a–h) and Late Triassic specimens (i–s). IRM acquisition curves and thermal demagnetization of three IRM curves (a–d, i–p); hysteresis loops (e–f, q–s); k–T curves (g–h) and a Day plot (t). In the Day plot, the red circles represent Early Triassic samples; the black circles represent Late Triassic samples.

strategy, rock magnetic measurements were conducted on representative samples from each stratum to determine the dominant carriers of the remanence magnetization. Isothermal remanent magnetization (IRM) acquisition curves were obtained from the samples using ASC Model IM−10−30 impulse magnetizers and JR−6A spinner magnetometers. Direct current magnetic fields of 2.7, 0.4, and 0.04 T, produced by ASC Model IM−10−30 impulse magnetizers, were applied to the Z-, Y-, and X-axes of the samples to identify hard, medium, and soft magnetic components (Lowrie, 1990). Then, samples with three-axis IRM were demagnetized in a TD−48 thermal demagnetization furnace and their thermomagnetic properties were measured with a 2G−755 superconducting magnetometer. Using a Kappabridge MFK1−FA with a CS−3 heating device, the samples were heated in argon to 700 °C and cooled to room temperature. Hysteresis loops were determined using the MicroMag Model 3900 Vibrating Sample Magnetometer. Information about grain-sizes of the minerals in the rock was obtained from a Day plot, which was constructed based on the hysteresis parameters (Day et al., 1977).

Based on the rock magnetic results, the samples were subjected to systematic magnetic cleaning using a stepwise alternating field, thermal or mixed demagnetization. Thermal demagnetizations were performed in an ASC−TD−48 furnace at low-temperature (<300 °C), followed by an interval at 50 °C, whereas at high-temperature, followed by a densified interval of 10−25 °C, and remanent magnetizations were measured using a 2G−755 magnetometer. For some specimens, alternating field demagnetizations were carried out at a demagnetized interval of 5−10 mT using the 2G−600 automatic AF degaussing system coupled with the 2G−755 magnetometer. Remanent magnetization directions were analyzed using principal component analysis (PCA) (Kirschvink, 1980), mean directions were calculated using Fisher statistics (Fisher, 1953), and demagnetization results were presented in orthogonal vector diagrams (Zijderveld, 1967) and equal-area projections. PMGSC software (written by Randy Enkin) was used to perform the analysis and to calculate the statistics in the paleomagnetic data.

4. Rock magnetism and SEM observations

Fig. 3a−h shows the rock magnetic results of the Early Triassic samples. The IRM acquisition curves (Fig. 3a, c) show a sharp increase in magnetism and reached quasi-saturation at less than 200 mT, which suggests the predominance of low coercivity magnetic minerals. This result is consistent with the characteristic of the hysteresis loops, which are narrow and closed near 250 mT (Fig. 3e and f). In three-axis IRM curves (Fig. 3b, d), the medium component accounted for greater than 65% and unblocked at

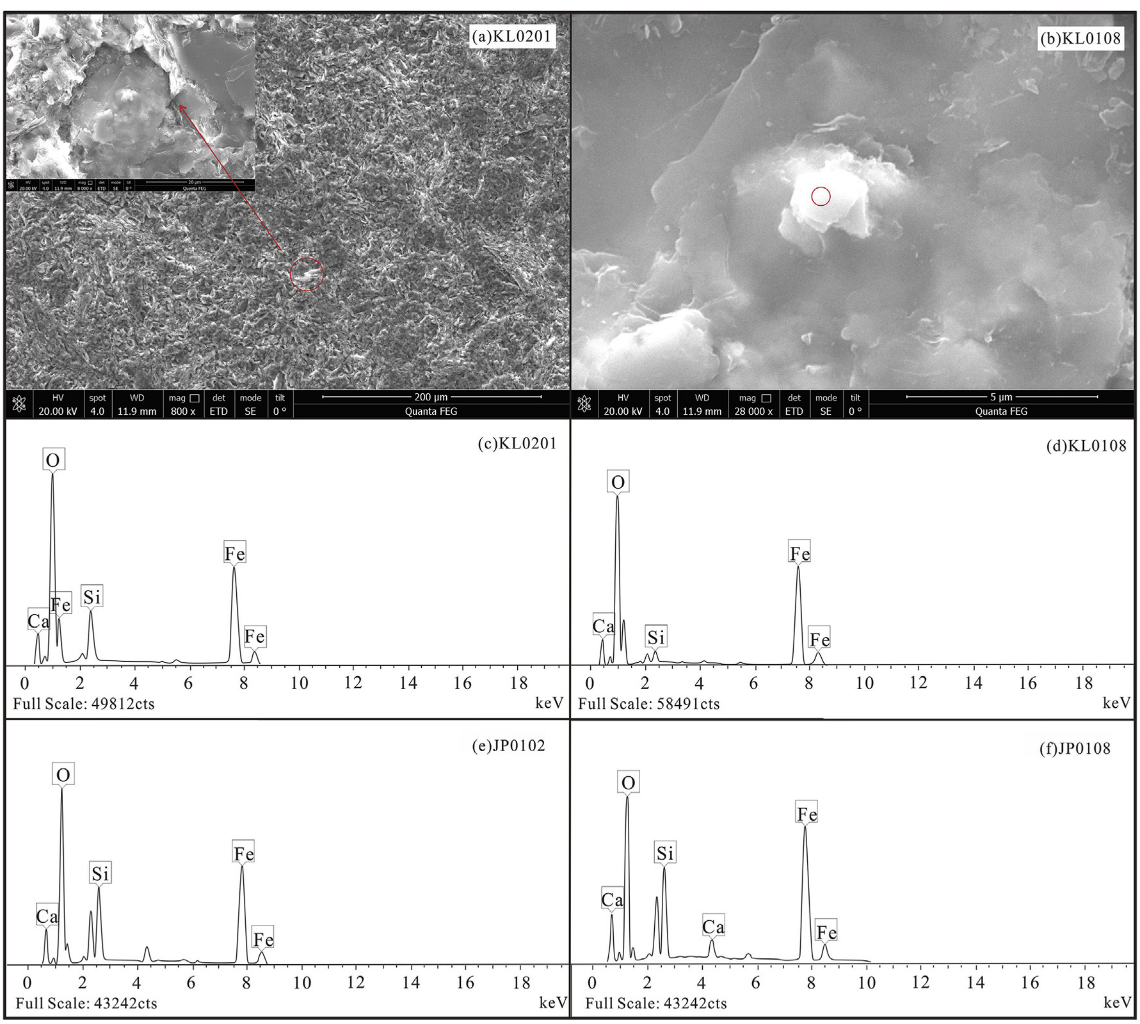

Fig. 4. Scanning electron microscopy (SEM) and energy dispersive spectroscopy (EDS) images of representative samples. The red circles of SEM (a, b) indicate spots analyzed using EDS; EDS results are listed in graphs c−f.

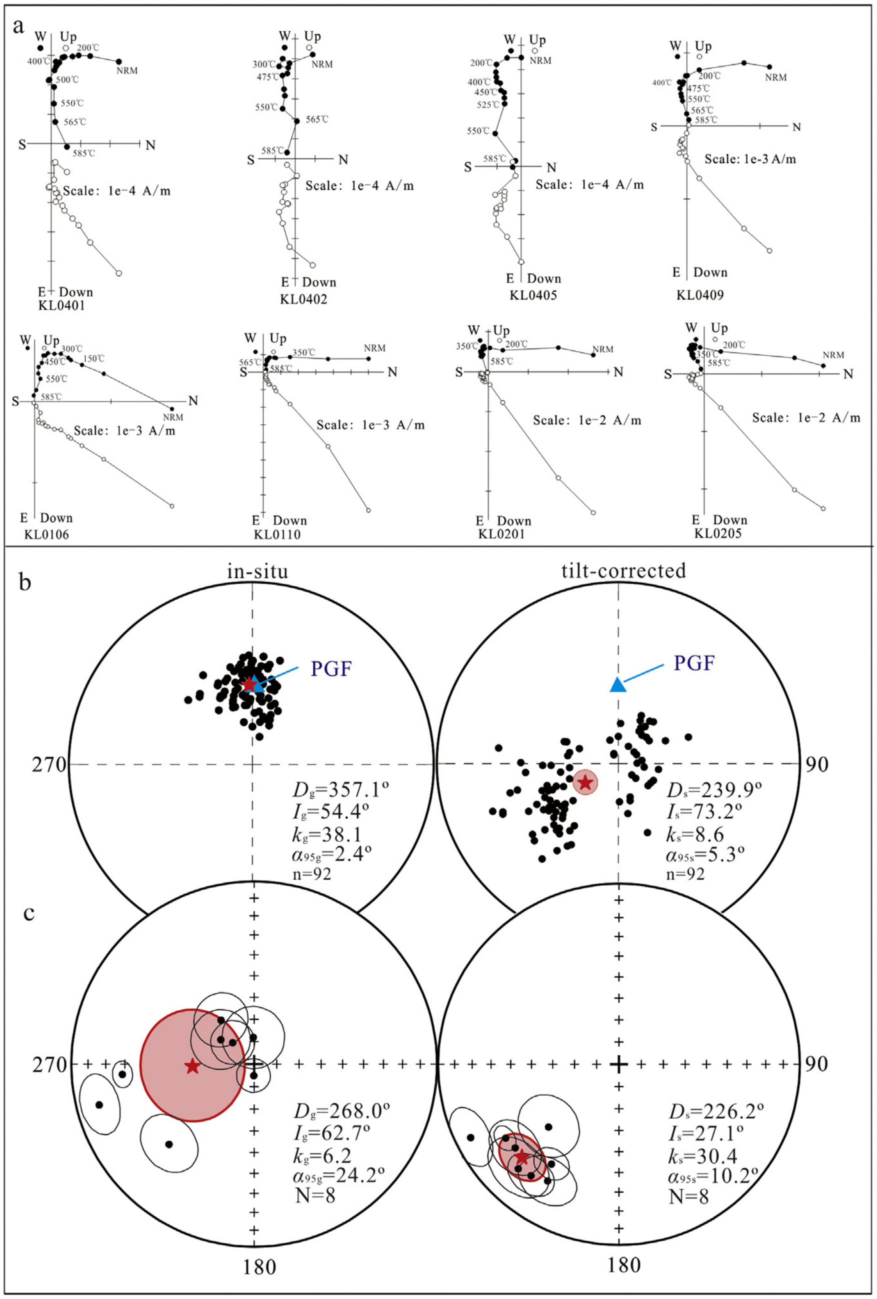

Fig. 5. Orthogonal vector plots of demagnetization behaviors in tilt-corrected coordinates from specimens representative of the Early Triassic (open circles portray vector endpoints projected onto the vertical planes; solid circles portray horizontal planes) (a). Equal-area projections in geographic coordinates (left) and stratigraphic coordinates (right) (open circles: upper hemisphere projections; solid circles: lower hemisphere projections) (b, c). Sample directions of the low-temperature/coercivity components (b). Site-mean directions of ChRM (c).

approximately 570 °C. Also, the thermomagnetic curves (Fig. 3g and h) indicated unblocking temperatures of magnetic carriers at ~580 °C. Taken together, these results suggest that the dominant magnetic carrier in the Early Triassic samples is magnetite.

Based on magnetic coercivity and unblocking temperature, the Late Triassic samples can be divided into two groups (Fig. 3i–s). (Group 1) The IRM curves of the Jiapila and Bagong samples (Fig. 3i, k) show a rapid increase in values before 200 mT. Moreover, the hysteresis loops (Fig. 3q and r) are narrow and closed near 500 mT, which indicates that the major magnetic minerals are low-coercivity minerals. The three-axis IRM (Fig. 3j, l) indicates that soft and medium components finally unblocked at 580 °C. Thus, the magnetic minerals in these samples are dominated by magnetite. (Group 2) The IRM acquisition curves of the Bilila samples (Fig. 3m, o) rise steeply in a low magnetic field (<250 mT), but the curves fail to saturate, even at 2700 mT. And the hysteresis loops (Fig. 3s), showing "wasp waist" and "goose-neck" shape, indicates that the major magnetic minerals are high-coercivity minerals. The three-axis IRM curves (Fig. 3n, p) indicate that medium and hard components were dominant and were unblocked at 670 °C. We infer that the dominant remanence carrier is hematite.

The Day plot enables estimation of the grain size of the magnetic minerals (Day et al., 1977). Eight representative samples from the Upper and Lower Triassic rocks were used for such analyses. The coercivity of remanence (H_{cr}) was calculated based on the backfield demagnetization of the saturation remanence (M_{rs}). The boundaries of magnetic grains are as follows (Day et al., 1977; Dunlop, 2002): $H_{cr}/H_c \leq 1.5$ and $M_{rs}/M_s \geq 0.5$ where the magnetic grains are single-domain (SD), and $H_{cr}/H_c \geq 5.0$ and $M_{rs}/M_s \leq 0.02$ where the magnetic grains are multi-domain (MD); the zone between SD and MD represents the pseudo-single-domain (PSD). As shown in Fig. 3t, all magnetic minerals lie within the PSD grain-size region.

To further clarify the textural relationships and diagenetic conditions of the magnetic minerals, polished thin sections of representative samples were examined using an FEI Quanta 400 FEG scanning electron microscope (SEM) at 20 kV. Energy dispersive spectrometer (EDS) analysis was subsequently conducted to obtain compositional information using an OXFORD IE 350 at the State Key Laboratory of Continental Dynamics, Northwest University (Xi'an, China). No obvious internal fracturing or oxidized edges of the magnetic mineral particles could be observed under SEM, which suggests that these magnetic minerals were not subjected to substantial stress (Fig. 4a and b). Pyrrhotite may not exist in these samples, because no strawberry-like mineral was found and no sulfur was detected with EDS. The EDS analysis also indicated that the magnetic minerals contained high oxygen and iron content (Fig. 4c–f). These results combined with the rock magnetic result suggest that the magnetic carriers in the Kanglu and Jiapiela formations are magnetite.

5. Paleomagnetic results

5.1. Results from the Early Triassic rocks

Fig. 5a shows demagnetization curves with two components of magnetization. At the beginning of demagnetization (temperature ≤ 300 °C, NRM ≤ 30 mT), the intensity of the remanent magnetization shows significant decay, and the low-temperature/coercivity components were erased. The directions of remanent magnetization changed after 350 °C and 30 mT, and the high-temperature/coercivity components decayed toward the origin from 475 °C to 585 °C.

Low-temperature (coercivity) was displayed by 92 specimens out of 112 demagnetized specimens. The mean direction of the low-temperature/coercivity components was $D = 357.1°$, $I = 54.4°$, $k = 38.1$, $\alpha_{95} = 2.4°$, $n = 92$ in geographic coordinates (Fig. 5b). This direction is close to the present geocentric axial field direction in this region (0°, 53.1°), suggesting that it might represent viscous remanent magnetization corresponding to the present geomagnetic field (PGF).

We obtained characteristic remanent magnetizations (ChRMs) from all sites of Lower Triassic rocks, including three sites in the Yingshuiquan Formation and five sites in the Kanglu Formation. Mean directions defined by less than five specimens with $k < 10$, and $\alpha_{95} > 15°$ were omitted to meet the Van der Voo (1990) reliability criteria. Fig. 5c and Table 1 show the high-temperature/coercivity directions of the Lower Triassic sedimentary rocks. The site-mean directions in the tilt-corrected coordinates ($D = 226.2°$, $I = 27.1°$, $k = 30.4$, $\alpha_{95} = 10.2°$, $N = 8$ sites) cluster much more closely than those in-situ ($D = 268.0°$, $I = 62.7°$, $k = 6.2$, $\alpha_{95} = 24.2°$, $N = 8$ sites). In addition, the data set passed the McElhinny fold test (1964) ($k_s/k_g = 30.4/6.2 = 4.9$, a critical value of 3.70 at a 99% confidence level), and the optimal concentration was reached at a 110.1% ± 10.2% unfolding percent age with a 95% confidence level (Watson and Enkin, 1993), indicating that the ChRM was acquired pre-folding (Fig. 7). As discussed in Section 2.1, the main deformation phase proceeded prior to the Late Triassic. This new direction is consistent with previously published the Late Paleozoic result in the region (Cheng et al., 2012a), and bears no resemblance to any younger result obtained from the NQB. Thus, we conclude that the ChRMs of eight sites record the Early Triassic primary remanence.

5.2. Results from the Late Triassic rocks

Orthogonal vector diagrams of the Late Triassic specimens exhibited two components of magnetic remanence (Fig. 6a). Samples (95 out of 114) with low-temperature or coercivity were demagnetized with an applied temperature below 300 °C or an alternating field of 20 mT. The mean direction of demagnetization was $D = 356.6°$, $I = 49.9°$ ($k = 8.1$, $\alpha_{95} = 5.4°$, $n = 95$) at the sample level in geographical coordinates (Fig. 6b). The individual directions of the low temperature (coercivity) component cluster well around the PGF in the study area at 0° and 53.6° suggesting that viscous remanent magnetization might have been recently-acquired.

The high-temperature or coercivity components of magnetization contained magnetite. Such samples were similar to the samples that contained hematites, and decayed toward the origin from 400 to 680 °C with an alternating field of 40–90 mT (Fig. 6a, Table 2). The overall mean direction calculated at nine sites (70 specimens) of the Jiezha Group was $D = 12.7°$, $I = 61.4°$ ($k = 6.6$, $\alpha_{95} = 21.7°$) in-situ, and $D = 7.0°$, $I = 31.9°$ ($k = 23.4$, $\alpha_{95} = 10.9°$)

Table 1
Characteristic remanences for the Lower Triassic sedimentary rocks from the NQB.

Site No.	Bedding attitude		n./N	In situ		Tilt corrected		α_{95} (°)	k	Pole position	
	Dd.	Dip (°)		D_g (°)	I_g (°)	D_s (°)	I_s (°)			λ_p (°N)	ϕ_p (°E)
YS/01	25	71	11/13	315.2	76.9	218.4	23.0	9.7	23.1	−31.5	41.4
YS/02	25	71	13/16	313.1	62.0	231.1	27.2	11.8	13.3	−21.6	32.7
YS/03	25	71	5/9	305.7	71.9	224.1	21.3	13.2	34.5	−28.7	35.8
KL/01	218	51.5	8/18	180.3	84.6	214.0	34.1	7.5	55.5	−28.4	49.9
KL/02	218	51.5	12/16	359.5	78.5	228.5	47.0	13.8	10.9	−12.9	44.3
KL/03	154	29	11/22	226.5	36.4	211.4	25.3	11.8	15.9	−34.3	49.0
KL/04	164	50	9/9	265.2	29.1	236.9	26.2	5.1	102.8	−18.0	28.1
KL/05	164	50	5/9	255.0	14.1	243.7	9.8	10.8	51.1	−18.6	16.4
Sites mean			74/8	268.0	62.7	226.2	27.1	24.2	6.2	−24.9	36.5
								10.2	30.4		

Notes: Site No., site number; Dd., dip direction; n./N, samples used to calculate the direction/number of demagnetized samples; for sites-mean direction, n/N, samples used to calculate the mean-direction/number of the sites to calculate the mean-direction; D_g, I_g, D_s, I_s, declination and inclination in situ and after tilt-coordinates; λ_p and ϕ_p, latitude and longitude of the corresponding VGP in stratigraphic coordinates; α_{95}, the radius of the cone of the 95% confidence for mean direction; k, precision parameter.
(1) McElhinny's fold test (1964): $N = 8$, $k_s/k_g = 30.4/6.2 = 4.9 > F(2 \times (n_2 - 1)\,(n_1 - 1)) = F(14, 14) = 3.70$, fold test is positive at the 99% confidence level.
(2) Watson and Enkin's fold test (1993): optimum concentration at (110.1 ± 10.2)% unfolding percentage.

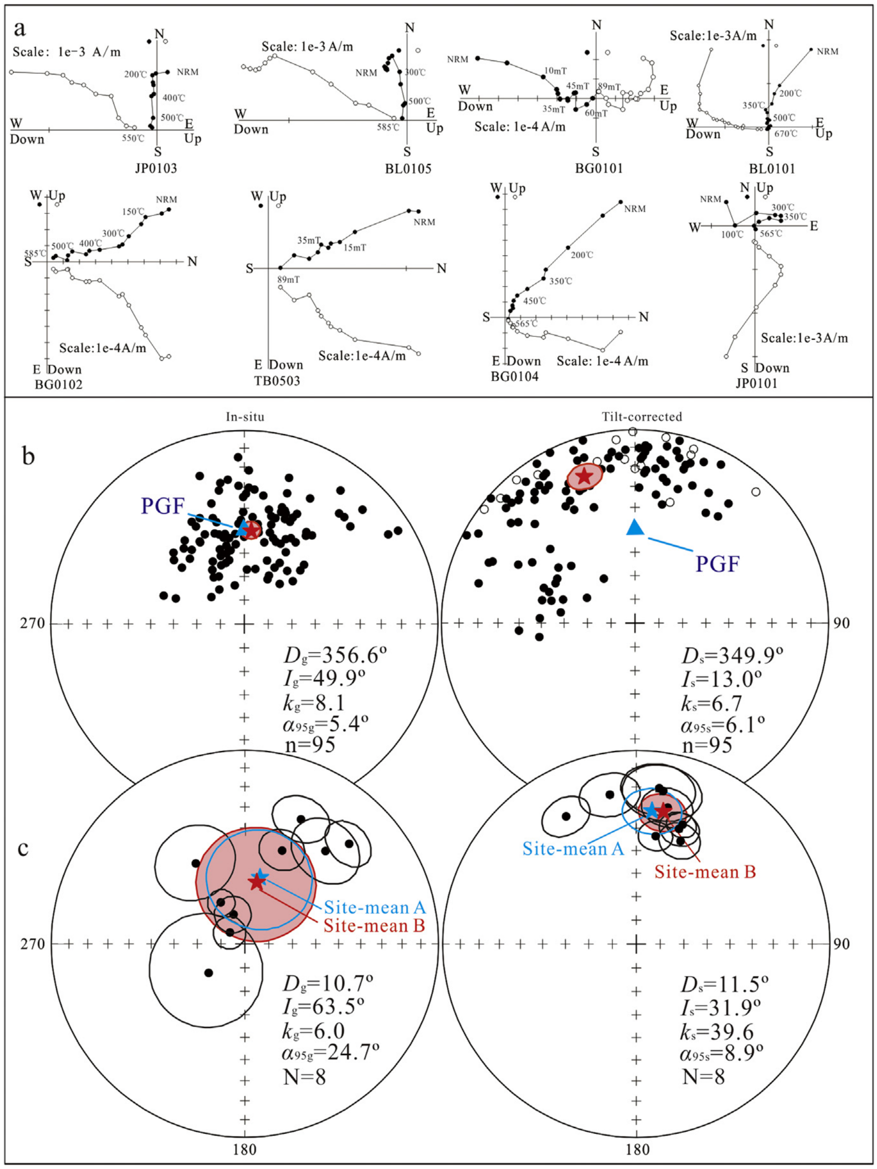

Fig. 6. Orthogonal vector plots of demagnetization behaviors in tilt-corrected coordinates from specimens representative of the Late Triassic (open circles portray vector endpoints projected onto the vertical planes; solid circles portray horizontal planes) (a). Equal-area projections in geographic coordinates (left) and stratigraphic coordinates (right) (open circles: upper hemisphere projections; solid circles: lower hemisphere projections) (b, c). Sample directions of the low-temperature/coercivity components (b). Site-mean directions of ChRM (c).

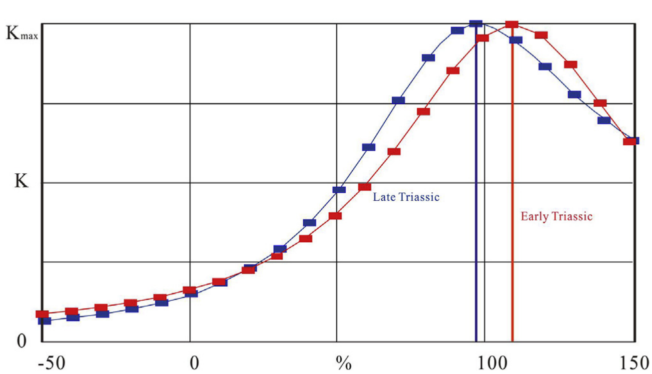

Fig. 7. After plunging fold correction, increment unfolding analysis using Watson and Enkin's methods (1993). Results for the Early Triassic (red line), and the Late Triassic (blue line).

after tilt correction (site-mean-A). The group-mean direction of BL05 was located >30° from site-mean-A, indicating that this direction might imply transitional field behavior, therefore, it was discarded from site-mean calculations. After excluding the anomalous direction, the mean of the remaining eight sites was $D = 10.7°$, $I = 63.5°$ ($k = 6.0$, $\alpha_{95} = 24.7°$) in-situ, and $D = 11.5°$, $I = 31.9°$ ($k = 39.6$, $\alpha_{95} = 8.9°$) after tilt correction (site mean-B). The stepwise unfolding correction indicated that the mean direction reached the highest precision parameter at 99.6% with a 95% confidence level (with uncertainties from 84.8% to 114.4%) (Watson and Enkin, 1993). The site-mean-B direction passed McElhinny's fold test (1964) at a 99% confidence level ($k_s/k_g = 39.6/6.0 = 6.6$, critical value = 3.70). As McFadden's fold test (1990) at a 99% confidence level ($\xi_2 = 7.297$ before, and $\xi_2 = 0.785$ after tilt correction, critical value $\xi = 4.562$), this indicated that the remanent magnetization was obtained before the folding of the strata. Furthermore, the folding might have occurred during Late Triassic to Early Jurassic

Table 2
Characteristic remanences for the Upper Triassic sedimentary rocks from the NQB.

Site No.	Bedding attitude		n/N	In situ		Tilt corrected		α_{95} (°)	k	Pole position	
	Dd.	Dip (°)		D_g (°)	I_g (°)	D_s (°)	I_s (°)			λ_p (°N)	ϕ_p (°E)
BG/01	45	72	5/13	231.9	70.8	23.1	42.1	8.1	90.2	67.7	202.2
BL/01	35	45	8/11	338.2	76.4	20.8	37.1	7.7	52.7	67.3	213.1
BL/02	21	44	11/14	307.8	81.9	10.3	43.2	6.7	47.4	77.4	224.7
BL/03	309	53	6/18	40.8	35.8	9.9	21.9	14.0	23.9	65.5	248.4
BL/04	297	57	8/12	45.8	26.0	13.0	28.8	9.4	35.7	67.9	237.2
BL/05	282	62	8/12	21.4	46.3	331.0	26.0	9.1	38.0	56.8	331.7
BL/06	282	62	9/14	24.2	29.4	350.0	23.1	10.8	23.7	66.1	297.2
JP/01	45	47	8/10	330.4	69.9	21.1	35.0	5.7	95.4	66.1	215.3
JP/02	45	47	7/10	328.7	49.2	8.3	20.6	13.0	22.5	65.3	252.5
Site-mean A			70/9	12.7	61.4	7.0	31.9	21.7 10.9	6.6 23.4	72.4	250.2
Site-mean B			62/8	10.7	63.5	11.5	31.9	24.7 8.9	6.0 39.6	70.3	238.0

Notes: see Table 1 for the details.
(1) McElhinny's fold test (1964) is positive both at 95% and 99% confidence level, $k_s/k_g = 39.6/6.0 = 6.6 > F(2 \times (n_2 - 1)(n_1 - 1)) = 2.48$ at the 95% point and 3.70 at the 99% point.
(2) McFadden's fold test (1990) is positive at the 95% confidence level, $\xi_2 = 4.608$ before and $\xi_2 = 0.579$ after tilt correction, critical ξ, at 95% = 3.298.
(3) McFadden's fold test (1990) is positive at the 99% confidence level, $\xi_2 = 7.297$ before and $\xi_2 = 0.7853$ after tilt correction, critical ξ, at 99% = 4.562.
(4) Watson and Enkin's fold test (1993): optimal concentration at (99.6 ± 14.8) % unfolding percentage.

periods, as discussed in Section 2.2, and the ChRMs are significantly different from the paleomagnetic features of younger rock units. Therefore, we suggest that this component has a primary origin.

6. Discussion

6.1. Reliability of ChRM from Triassic rocks of the NQB

The ChRM derived from sedimentary rocks might be affected by inclination shallowing, mainly due to mechanical compaction of the sediments during diagenesis (King, 1955; Jackson et al., 1991; Kodama and Sun, 1992). Huang (2012) proposed a method to detect inclination shallowing for a small number of samples. For the Early Triassic samples, our results using this method indicated no obviously inclination shallowing ($\theta < 80°$ and $\Delta\theta<0°$) (Table 3). As the commonly applied inclination flattening correction for Asia is 0.5–0.6 (Torsvik et al., 2012; Wu et al., 2017a; Zhang et al., 2018). Wu et al. (2017a) compared coeval igneous paleomagnetic poles that are not affected by the shallowing error with the poles from clastic rocks. They found inconclusive evidence for inclination flattening (IF) effects on the clastic paleopoles during some periods/epochs. Huang et al. (2018) accepted paleopoles from clastic rocks without IF correction when the pole positions were comparable with coeval paleomagnetic results from volcanic rocks of the same age. Because our Early Triassic result without IF correction is consistence with the results derived from ~250 Ma volcanic rocks in same region which are supposed to be immune with inclination shallowing (Zhang, 2017). Therefore, further we discuss two possibilities to interpret our Lower Triassic result with and without IF correction applied.

Table 3
Inclination shallowing of the Triassic sedimentary rocks.

Geologic time	N	D_{V_2} (°)	D_{ave} (°)	θ (°)	Λ (°)	θ_c (°)	$\Delta\theta$ (°)
Early Triassic	8	175.6	226.2	51.2	14.3	82.3	−31.1
Late Triassic	8	108.0	11.5	96.5	17.3	80.9	15.6
Early Triassic: $\theta < 80°$ and $\Delta\theta<0$, no inclination shallowing							
Late Triassic: $\theta > 80°$ and $\Delta\theta>0$, inclination shallowing							

Notes: N, Number of sites; D_{V_2}, declination corresponding to the direction matrix eigenvector V_2 of directional matrix; D_{ave}, mean declination calculated from the directions; θ, the angle between D_{V_2} and D_{ave}; θ_c, the 95% upper limit value of the cumulative distribution of θ values; $\Delta\theta$, $\theta-\theta_c$.

The Early Triassic paleomagnetic results from the Yingshuiquan and Kanglu formations met six of the seven criteria (Van der Voo, 1990). The age of the sampled strata was determined based on stratigraphic sequences, paleontological assemblages, and detrital zircon dating (Xie et al., 2018). Rock magnetic experiments and demagnetization procedures suggested that ChRM was mainly carried by PSD magnetite, which is a stable remanent magnetization carrier. The demagnetization curves in our study exhibit both low and high temperature or field components of the magnetic remanence. ChRMs that passed fold tests at the 99% confidence level were obtained from eight sites (74 samples). The mean ChRM direction bears no resemblance to more recently published results from the NQB. Therefore, we propose that the ChRMs record the primary magnetizations, corresponding to a paleopole at 24.9 °N, 216.5 °E ($A_{95} = 8.2°$), and a paleolatitude of 14.3°S±8.2° without IF correction and 27.1°S±8.2° with IF correction 0.5. This paleopole is the first paleomagnetic result from a field tests in the Lower Triassic strata of the NQB.

The paleogeographic position of the NQB in the Late Triassic is poorly reconstructed because of the relative scarcity of paleomagnetic data (Ye and Li, 1987; Lin and Watts, 1988; Song et al., 2012, 2015). We reevaluated Late Triassic paleomagnetic data and listed them in Table 4. Ye and Li (1987) and Lin and Watts (1988) conducted preliminary research on the Upper Triassic strata of the NQB. We did not use these results because they were obtained with pre-modern paleomagnetic equipment and analysis techniques or lacked detailed sampling and demagnetization information. Song et al. (2012) reported a paleopole from Upper Triassic sandstone at the northern margin of the LSLS. We did not use this result because the authors did not discuss inclination shallowing.

Recently, Song et al. (2015) obtained ChRMs from volcanic rocks of the Jiapila Formation in the Tuotuohe area, which passed reversal and fold tests. In our analysis we used their new pole (64.5°N, 177.8°E, $A_{95} = 6.4°$) that provides a paleolatitude of 29.7°N±6.4°. We note that the mean inclination we obtained from the sedimentary rocks is shallower than that of coeval volcanic rocks in the same area (Song et al., 2015). The IF detection method of Huang (2012) suggests that shallowing might occurred in our study of Late Triassic sedimentary strata ($\theta > 80°$ and $\Delta\theta>0°$) (Table 3). We therefore applied the E/I method of Tauxe and Kent (2004) to

Table 4
Paleomagnetic data from the Late Paleozoic to the Early Mesozoic of the NQB and the Triassic paleomagnetic data form its adjacent blocks.

Sampling location	GPS		Age (Ma)	Rock units	Lithology	n/N	Paleopole			Tests	Q	Paleolat. (°)	Reference
	Lat. (°N)	Lon. (°E)					λ_p (°N)	ϕ_p (°E)	α_{95} (°)				
Results from NQB, reference point (33.7°N, 86.9°E)													
Yanshiping	33.6	92.1	J_3	Suowa Fm.	limestones	6/59	83.3	268.3	7.6	FT	6	27.0 ± 7.6	Cheng et al. (2012b)
Yanshiping	33.6	92.1	J_3	Suowa Fm.	limestones	20/191	72.4	318.6	5.1	RT, FT	7	21.9 ± 5.1	Yan et al. (2016)
Mean			J_3	Suowa Fm.		26/250	75.0	315.2	4.5			23.1 ± 4.5	
Yanshiping	33.6	92.1	J_2	Buqu Fm.	limestones	5/37	75.1	308.5	8.9	FT	6	22.1 ± 8.9	Cheng et al. (2012b)
Yanshiping	33.6	92.1	J_2	Buqu Fm.	limestones	27/245	68.9	313.8	2.8	RT	6	18.2 ± 2.8	Yan et al. (2016)
Mean			J_2	Buqu Fm.		32/282	69.9	313.1	2.7			18.9 ± 2.7	
Tuotuohe	34.1	92.4	T_3	Jiapeila Fm.	volcanics	29/238	64.5	177.8	6.4	RT, FT	7	29.7 ± 6.4	Song et al. (2015)
Tuotuohe	34.1	92.4	T_3	Jiezha Gp.	sediments	8/62	80.4	185.2	7.5	RT	6	31.8 ± 7.5	This study
Mean			T_3	Jiezha Gp.		37/300	68.1	179.9	5.6			29.9 ± 5.6	
Rejuechaka	33.7	86.9	T_1	Yingshuiquan Fm., Kanglu Fm.	sediments	8/74	24.9	216.5	8.2	FT	6	-14.3 ± 8.2	This study
Nuoribanabao	33.9	91.9	P_3	Nayixiong Fm.	lavas	30/253	10.6	9.4	4.0	FT	6	-16.2 ± 4.0	Zhang (2017)
Nuoribanabao	33.9	91.9	P_3	Nayixiong Fm.	lavas	28/184	13.6	2.4	5.6	FT	6	-12.0 ± 5.6	Ma et al. (2019)
Mean			P_3	Nayixiong Fm.		58/437	11.0	7.4	3.2			-14.8 ± 3.2	
Nuoribanabao	33.9	91.9	P_2	Jiushidaoban Fm.	limestones	5/42	1.0	24.1	14.6	FT	5	-22.9 ± 14.6	Cheng et al. (2013)
Tuotuohe	34.1	92.4	P_1	Kaixinling Gp.	lavas	14/129	21.7	232.9	8.9	FT	6	-25.8 ± 8.9	Song et al. (2017)
Tuotuohe	34.1	92.4	C_2	Zarigen Fm. Nuoribagaribao Fm.	limestones, sandstones	16/127	25.7	241.5	2.2	CT	6	-25.9 ± 2.2	Yang et al. (2017)
Triassic results from the Lhasa block; reference point (33.7°N, 86.9°E)													
Dibucuo	30.9	84.7	T_3	Zhulung and GyangRang Fm.	limestones	6/37	19.6	211.8	10.7	FT	6	-15.2 ± 10.7	Zhou et al. (2016)
Dibucuo	30.9	84.7	T_{1-2}	Garing Co Fm.	limestones	8/47	18.9	208.4	3.9	RT, FT	7	-13.4 ± 3.9	Zhou et al. (2016)
Triassic results from Tarim; reference point (33.7°N, 86.9°E)													
-	41.8	80.5	210	-	-	8/-	52.1	166.8	7.0	RT	5	31.8 ± 6.7	Huang et al. (2018)
-	52.8	74.9	250	-	-	5/-	53.9	175.4	8.0	RT	5	27.5 ± 8.0	Huang et al. (2018)

Notes: Sampling location, paleomagnetic sampled locality; Age (Ma), the strata age of the study area; Rock units, the name of sampled strata; Gp., Group; Fm., Formation; n/N, sites/samples used to calculate the paleopole; α_{95}, the 95% confidence circle about the reference pole; Tests: RT, FT, CT, positive fold test, reverse test and conglomerate test, respectively; Q: number of quality criteria proposed by Van der Voo (1990) which the data met; Criteria 1 (well-determined sampled rock age), 2 (sufficient number of available samples: $N > 24$, $k \geq 16$ and $\alpha_{95} \leq 16°$), 3 (reasonable demagnetization steps), 4 (field test), 5 (structural control), 6 (the presence of reversals) and 7 (no resemblance to paleopoles of any younger age). Plaleolat., the paleolatitude calculated from paleopole from published literature and this study at the reference site (33.7°N, 86.9°E). For the Yanshiping Gp., we only list the results isolated from the limestone which seems immune the inclination shallowing.

correct the inclination shallowing (Fig. 8a). The corresponding shallowing flattening factor ($f = 0.5$) produced after 1000 bootstrap simulations gave a mean inclination of 52.5° within a 95% confidence limit (Fig. 8b and c). This mean inclination after correction is consistent with the mean inclination of the coeval volcanic rocks (53.0°±5.5°). The site-mean directions from both sedimentary and volcanic rocks were combined to calculate the Late Triassic paleolatitude of the NQB using Fisher statistics. The overall direction (Fig. 9), calculated from 29 volcanic (Song et al., 2015) sites and eight sedimentary sites after E–I correction in the Tuotuohe area, was $D = 26.1°$, $I = 51.6°$ ($k = 23.6$, $\alpha_{95} = 5.0°$) after tilt correction. Therefore, we proposed a new Late Triassic paleopole located at 68.1°N, 179.9°E ($A_{95} = 5.6°$), corresponding to a paleolatitude of ~29.9°N±5.6°, and used it for further discussion.

6.2. Rapid northward motion of the NQB during the Triassic Period

To gain a better understanding of the kinematic process of northern Qiangtang Block, available paleomagnetic results from the Late Paleozoic to the Early Mesozoic were reviewed (Table 4). These data show that the NQB was located in the subtropical southern hemisphere during the Late Paleozoic Era (Cheng et al., 2012a, 2013; Song et al., 2017; Yang et al., 2017; Zhang, 2017; Ma et al., 2019). Two kinds of paleogeographic models have been proposed for this interval. The typical markers of Gondwanan affinity—mostly glacial-marine deposits and cold-water biota—were preserved in Permian rocks, which implied that the NQB was connected with Gondwana or located in the northern margin of Gondwana in that period (Wang, 1984; Pullen and Kapp, 2014). On

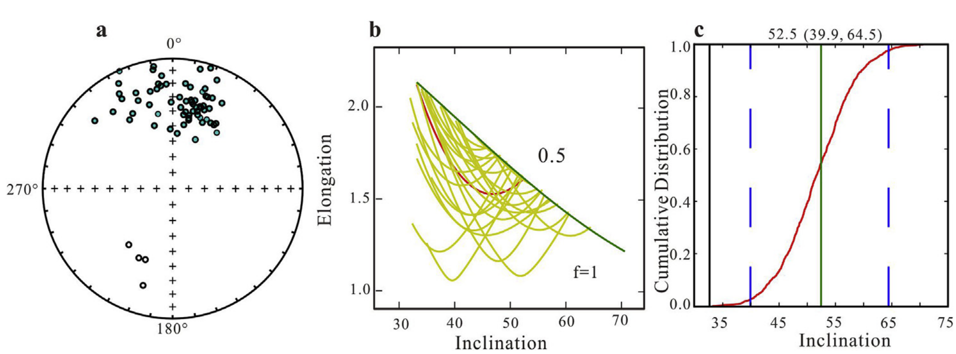

Fig. 8. Results of the E/I method (Tauxe and Kent, 2004) to correct the inclination shallowing of the paleomagnetic directions of the Jiezha Group. Paleomagnetic directions of the Jiezha Group in equal area projection (stratigraphic coordinates) (a). Elongation versus inclination for the TK03. GAD model (green line) and for the Jiezha Group (red line) for different values f. (b) Cumulative distribution of crossing points from 1000 bootstrapped datasets (c). The most frequent inclination is 52.5°, and the 95% confidence bounds are 39.9°–64.5°.

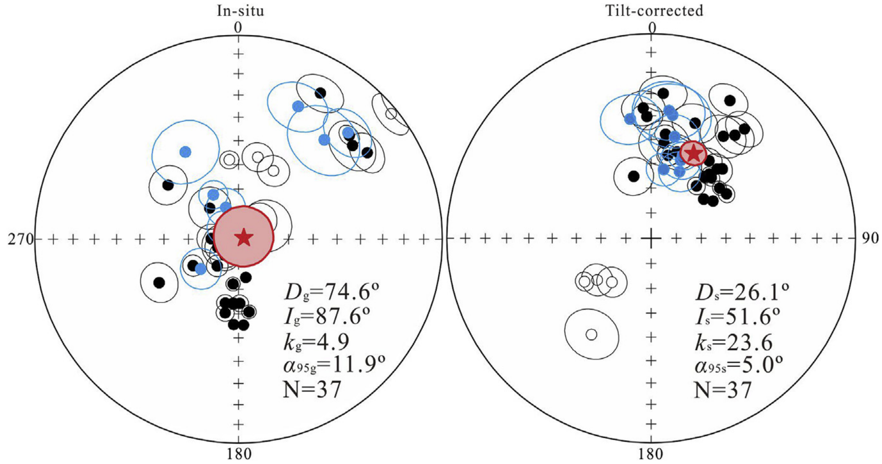

Fig. 9. Equal-area projections showing sites-mean directions of the ChRM component from the Upper Triassic Jiezha Group in geographic coordinates (left) and stratigraphic coordinates (right). The blue circles represent the sedimentary results after E/I correction; the black circles represent the volcanic results from Song et al. (2015); the red five-point stars represent the overall direction.

the other hand, Paleozoic ophiolites were found in the Longmu Co–Shuanghu suture and in the Bangong–Nujiang suture, which suggests that the NQB had to rift from the northern margin of Gondwana in the Late Paleozoic Era (Liu et al., 2014; Fan et al., 2017, 2018; Wu et al., 2017b; Zeng et al., 2018). In both models above, the NQB remained in mid-low latitudes of the southern hemisphere during the Late Paleozoic. Our results indicate that the block started its significant northward drift from the southern to the northern hemisphere not earlier than the beginning of the Early Triassic. Stratigraphic, geochemical, and isotopic analyses have indicated that the Yingshuiquan and Kuanglu formations accumulated during an event of extensional tectonic activity (Zhang et al., 2002; Li et al., 2007; Zhang and Tang, 2009; An, 2014; Qu et al., 2015; Xie et al., 2018) that might indicate an active plate tectonic movement.

Close paleolatitude values for northern Qiangtang and Tarim blocks indicate that the NQB approached Eurasia in the Late Triassic (Fig. 10). This interpretation is supported by extensive geological and paleontological evidence (Metcalfe, 2013; Wu et al., 2017b). For example, Late Triassic turbidite sequences and molasse were observed along the northern margin of the NQB (Weislogel, 2008; Ding et al., 2013). The transformation of the depositional environment during the Late Triassic to the Early Jurassic (Chen and Wang, 2009; Fu et al., 2013), as well as the unique weathered paleocrust, were preserved in the northern Qiangtang Block and in adjacent terrains. All these characteristics suggest that the northern Qiangtang Block had approached Eurasia (Fu et al., 2010; Wang and Fu, 2018).

Based on the paleomagnetic results, we suggest a three-stage northward drift of the NQB. (1) The block was located in the subtropical southern hemisphere before the Early Triassic. (2) During the Triassic Period, the block drifted rapidly northward from the southern to the northern hemisphere. (3) The block approached Eurasia in the Late Triassic. We used zircon LA–ICP–MS dating of the Yingshuiquan Formation (249 Ma; Xie et al., 2018) and the Jiezha Group (208.5 Ma; Song et al., 2015) to estimate the total south-north movement of the NQB in the Triassic. The block moved at least 44.2°±7.3° in latitude (~4800 km) during a 40.5 Myr interval; that corresponds to an average drift rate of 11.85 cm/yr. Taken Tarim Block as reference paleopole, the NQB accompanied by a 15.8°±9.1° clockwise rotation during the Triassic Period. The

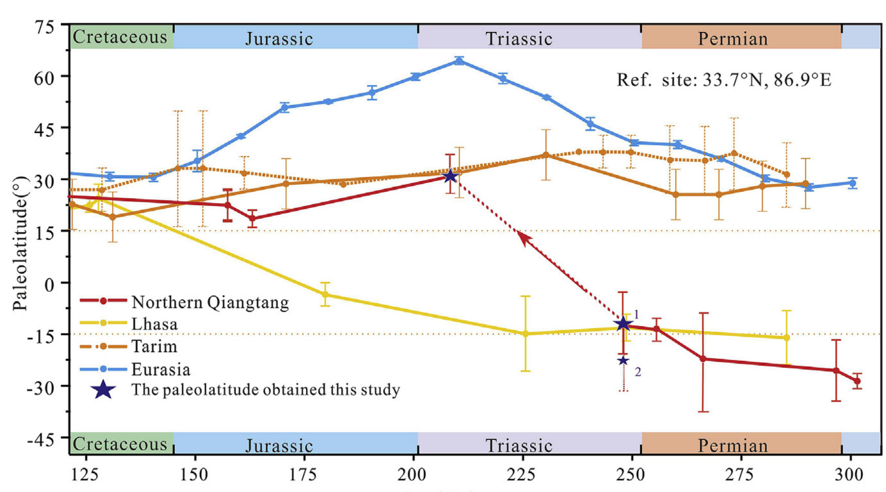

Fig. 10. Paleolatitude of the NQB and adjacent terrains during the Late Paleozoic and Early Mesozoic. For the paleolatitudes of NQB are from the sources referred in Table 4. Eurasian paleolatitudes: Torsvik et al. (2012); The Permian, Triassic and Early Jurassic paleolatitudes of the Lhasa are from Ran et al. (2012), Li et al. (2016b) and Zhou et al. (2016). The Tarim: Wu et al. (2017a) with inclination flattening correction (dashed line); Huang et al. (2018) without the correction (solid line).

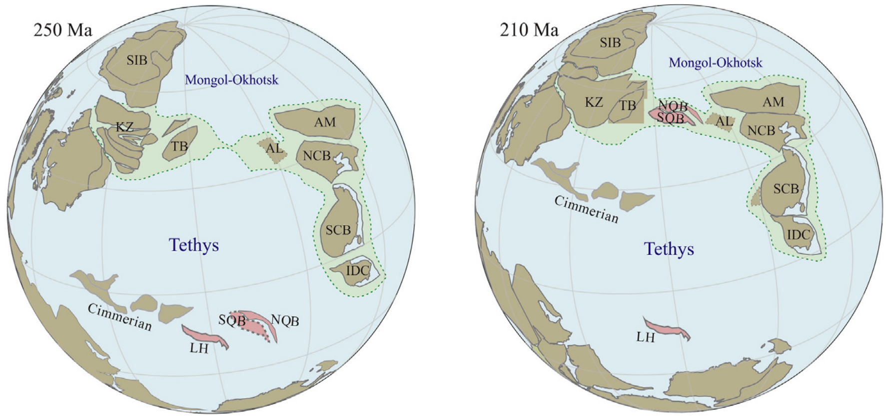

Fig. 11. Paleogeography of the NQB 250 Ma and 210 Ma, modified after reconstructions from Wu et al. (2017a,b). Data are from the sources referred in Fig. 10. Abbreviations: SIB–Siberia; KZ–Kazhakstan; TB–Tarim Block; AL–Alashan; AM–Amuria; NCB–North China Block; SCB–South China Block; IDC–Indochina; NQB–Northern Qiangtang Block; SQB–Southern Qiangtang Block; LH–Lhasa Block.

northward drift rate of the NQB was similar to that of several other blocks such as North China, South China, Lhasa, Baoshan, and Indochina blocks, which also experienced large S–N movements during the mid–late Paleozoic or the Mesozoic as they transferred from the margin of Gondwana to the vicinity of Eurasia (e.g., Xu et al., 2015; Zhao et al., 2015; Li et al., 2016b; Huang et al., 2018; Yan et al., 2018).

6.3. Constraints on evolution of the Tethyan ocean basin

The NQB is considered to be a key region for understanding the evolution of the Tethys Ocean. Our paleomagnetic results for the Triassic rocks from this block provide paleomagnetic constraints for paleogeographic reconstructions of Eurasia.

Early and Late Triassic NQB paleolatitudes were compared with coeval paleolatitudes in tectonic blocks of Tarim and Lhasa using a reference point located at 33.7°N, 86.9°E in the NQB (Fig. 10). For the Lhasa block, we used results in Zhou et al. (2016) to calculate the Triassic position because they are the only available Triassic data with relatively high Q factors ($Q \geq 5$). Early-Middle Triassic and Late Triassic paleopoles are situated 18.9°N, 208.4°E ($A_{95} = 3.9°$) and 19.6°N, 211.8°E ($A_{95} = 10.7°$), respectively, and correspond to paleolatitudes of ~13.4°S±3.9° and ~15.2°S±10.7°. For the Tarim Block, apparent polar wander paths (APWPs) were constructed using a running mean through different window sizes by weighting the paleomagnetic poles according to their reliability criteria indices $Q \geq 4$ (Wu et al., 2017a; Huang et al., 2018). We used the paleopoles, 52.1°N, 166.8°E ($A_{95} = 7.0°$) for the 210 Ma and 53.9°N, 175.4°E ($A_{95} = 8.0°$) for the 250 Ma, to calculated further. There is only one paleomagnetic data for the southern Qiangtang Block showed that the northern and southern Qiangtang Block had merged in the Late Triassic. We hypothesis that both northern and southern Qiangtang Block have almost similar kinematic features, which was shown to have a southern hemisphere paleolatitude during the Early Triassic times. For the NQB we used 250 Ma (24.9°N, 216.5°E, with $A_{95} = 8.2°$) and 210 Ma (68.1°N, 179.9°E, with $A_{95} = 5.6°$) paleopoles that yield paleolatitudes of 14.3°N ± 8.2° and 29.9°N ±5.6°, respectively, for the reference point to reconstruct the paleogeography further. In Fig. 10 we show two possible paleolatitudes for the Early Triassic: (1) a southern hemisphere latitude with no IF correction, (2) a southern hemisphere latitude with an IF correction of 0.5. Our preference is (1) because this result matches well with previously published results for earlier ages and positions of the Cimmerian terranes (Cheng et al., 2012a; Domeier and Torsvik, 2014; Zhang, 2017; Ma et al., 2019), although such result produces quite a high drift rate (11.85 cm/yr) during the Triassic.

Our results, summarized in Fig. 11, showed that the rapid drift of the NQB after the Early Triassic led to a drastic change in the configuration of the Tethys Ocean. This inference is supported by overlapping paleopoles from the northern Qiangtang and Lhasa blocks in the Early Triassic. A latitudinal difference of ~42° between northern Qiangtang and Lhasa blocks evolved between the Early and Late Triassic. The paleopole of the NQB was similar to that of the Tarim Block in the Late Triassic, whereas the paleolatitude difference was ~45.1° in the Early Triassic. Thus, based on the comparison of paleolatitude data described above, we infer that the Tethys Ocean was restructured very quickly in the Triassic Period.

7. Conclusions

We presented two new paleomagnetic poles from the Lower and Upper Triassic sedimentary strata of Raggyorcaka and Tuotuohe areas of the northern Qiangtang Block (NQB). Stepwise thermal/alternating field demagnetization demonstrated the presence of stable ChRMs in Early and Late Triassic samples. Both collections passed the fold tests at a 99% confidence level. By combining these results with previously published data, we reconstructed a northward drift of the northern Qiangtang Block of thousands of kilometers from the Early to the Late Triassic. We suggest that the average drift rate was very high compared to present day continental drift velocities.

Acknowledgments

Financial support for this study was jointly provided by the National Natural Science Foundation of China (Grant Nos. 91855211, 41421002, 41674070, 41702233, and 41774073), the Scientific Research Program Funded by Shaanxi Provincial Education Department (Grant No. 17JK0784), the Natural Science Foundation of Shaanxi Province of China (Grant No. 2017JQ4027), and the Natural Sciences and Engineering Research Council of Canada (NSERC grant RGPIN-2019-04780). We thank Academicians Rixiang Zhu and Lin Ding, Profs. M. Santosh, Baochun Huang and Yunpeng Dong, and Drs. Yonggang Yan and Jie Zhao. We also thank the editors and three anonymous reviewers who provided useful comments that led to improvement of the manuscript.

Appendix

Table A.1
The sedimentary directions after E/I correction and volcanic directions of Jiezha Group from the Tuotuohe area (34.1°N, 92.4°E) of Northern Qiangtang Block.

Site No.	D_s (°)	I_s (°)	α_{95} (°)	k	Site No.	D_s (°)	I_s (°)	α_{95} (°)	k	Site No.	D_s (°)	I_s (°)	α_{95} (°)	k
BG/01	23.1	61.0	8.1	90.2	T06	35.3	38.8	8.7	78.3	T19	40.9	62.3	3.5	251.3
BL/01	20.8	56.5	7.7	52.7	T07	211.8	−43.9	10.3	56.1	T20	41.4	57.3	2.4	779.7
BL/02	10.3	62.0	6.7	47.4	T08	232.4	−62.7	6.3	78.2	T21	29.8	23.5	6.9	77.5
BL/03	9.9	38.8	14.0	23.9	T09	39.1	35.3	7.5	105.0	T22	237.0	−58.1	3.7	171.3
BL/04	13.0	47.7	9.4	35.7	T10	59.5	54.8	3.4	266.2	T23	221.8	−66.5	6.0	163.5
BL/06	350.0	40.5	10.8	23.7	T11	20.9	39.6	8.4	83.9	T24	358.0	40.2	5.7	181.1
JP/01	21.1	54.5	5.7	95.4	T12	36.8	50.9	5.1	141.0	T25	40.5	30.4	7.1	73.2
JP/02	8.3	36.9	13.0	22.5	T13	356.5	36.4	7.7	52.7	T26	7.9	47.4	4.0	75.6
T01	344.3	64.3	7.7	76.7	T14	43.6	51.4	6.1	33.1	T27	16.7	53.7	7.3	69.3
T02	11.4	56.0	4.2	151.2	T15	44.8	55.7	3.4	266.2	T28	4.8	29.7	8.2	88.0
T03	26.7	52.4	4.3	144.3	T16	53.8	55.9	2.8	136.7	T29	7.7	51.2	9.5	50.7
T04	45.7	49.8	2.1	601.5	T17	59.0	61.1	2.0	663.0	Mean	26.1	51.6	5.0	23.6
T05	42.2	55.1	2.8	338.8	T18	53.4	63.8	1.7	1061.5					

Notes: D_s, I_s, declination and inclination after tilt-coordinates; α_{95}, the radius of the cone of the 95% confidence for mean direction; k, precision parameter. The results of BG, BL, JP which used for calculated the mean direction are from this paper; the results of T are from Song et al. (2015).

References

Aitchison, J.C., Ali, J.R., Davis, A.M., 2007. When and where did India and Asia collide? Journal of Geophysical Research 112 (B05423), 1–21.

Allégre, C.J., Courtillot, V., Tapponnier, P., Hirn, A., Mattauer, M., Coulon, C., Jaeger, J.J., Achache, J., Schärer, U., Marcoux, J., Burg, J.P., Girardeau, J., Armijo, R., Gariépy, C., Göpel, C., Li, T.D., Xiao, X.C., Chang, C.F., Li, G.Q., Lin, B.Y., Teng, J.W., Wang, N.W., Chen, G.M., Han, T.L., Wang, X.B., Den, W.M., Sheng, H.B., Cao, Y.G., Zhou, J., Qiu, H.G., Bao, P.S., Wang, S.C., Wang, B.X., Zhou, Y.X., Xu, R.H., 1984. Structure and evolution of the Himalaya-Tibet orogenic belt. Nature 307, 17–22.

An, X.Y., 2014. Analysis of Sedimentary Facies Characteristic and Provenance Upper Permian to Middle Triassic in the Northern Qiangtang, Tibet. M.S. thesis. China University of Geosciences, Beijing, p. 59 (in Chinese with English abstract).

BGMR, 1993. Regional Geology of Xizang(Tibet) Autonomous Region. Geological Publishing House, Beijing (in Chinese with English abstract).

Bian, Q.T., Zheng, X.S., Li, H.S., Sha, J.G., 1997. Age and tectonic setting of ophiolite in the Hoh Xil region Qinghai Province. Geological Review 43 (4), 347–355 (in Chinese with English abstract).

Calais, E., Vergnolle, M., San'kov, V., Lukhnev, K., Miroshnitchenko, A., Amarjargal, S., Déverchère, J., 2003. GPS measurements of crustal deformation in the Baikal-Mongolia area (1994-2002): Implications for current kinematics of Asia. Journal of Geophysical Research 108 (B10), 2501–2514.

Cao, Y., Sun, Z.M., Li, H.B., Pei, J.L., Liu, D.L., Lei, Z., Ye, X.Z., Zheng, Y., He, X.L., Ge, C.L., Jiang, W., 2019. New paleomagnetic results from Middle Jurassic limestones of the Qiangtang terrane, Tibet: constraints on the evolution of the Bangong-Nujiang ocean. Tectonics 38 (1), 215–232.

Chang, C.F., Zheng, H.L., 1973. Some tectonic features of the Mt. JolmoLungma area, southern Tibet, China. Science China Earth Sciences XVI (2), 257–265.

Chen, W.W., Zhang, S.H., Ding, J.K., Zhang, J.H., Zhao, X.X., Zhu, L.D., Yang, W.G., Yang, T.S., Li, H.Y., Wu, H.C., 2017. Combined paleomagnetic and geochronological study on Cretaceous strata of the Qiangtang terrane, central Tibet. Gondwana Research 41, 373–389.

Chen, X.W., Wang, J., 2009. Correlation of upper Triassic strata in Qiangtang basin, northern Tibet. Geology in China 36 (4), 682–693 (in Chinese with English abstract).

Chen, Y., Cogne, J.P., Courtillot, V., 1993. Cretaceous paleomagnetic results from western Tibet and tectonic implications. Journal of Geophysical Research 98 (B10), 17981–17999.

Cheng, X., Wu, H., Diao, Z., Wang, H., Ma, L., Zhang, X., Yang, G., Hong, J., Ji, W., Li, R., Chen, S., Zhao, Z., 2013. Paleomagnetic data from the Late Carboniferous–Late Permian rocks in eastern Tibet and their implications for tectonic evolution of the northern Qiangtang-Qamdo block. Science China Earth Sciences 56 (7), 1209–1220.

Cheng, X., Wu, H., Guo, Q., Hou, B., Xia, L., Wang, H., Diao, Z., Huo, F., Ji, W., Li, R., Chen, S., Zhao, Z., Liu, X., 2012a. Paleomagnetic results of late Paleozoic rocks from northern Qiangtang block in Qinghai–Tibet plateau, China. Science China Earth Sciences 55 (1), 67–75.

Cheng, X., Wu, H.N., Diao, Z.B., Wang, H.J., Zhang, X.D., Ma, Lun, Zhou, Y.N., Kang, W.W., Ji, W.H., Li, R.S., Chen, S.J., Zhao, Z.M., 2012b. Newpaleomagnetic result of Middle lateJurassic rocks from northern Qiangtang block, west China. Chinese Journal of Geophysics 55 (10), 399–409 (in Chinese with English abstract).

Dai, J.G., Zhao, X.X., Wang, C.S., Zhu, L.D., Li, Y.L., Finn, D., 2012. The vast proto-Tibetan plateau: new constraints from Paleogene Hoh Xil basin. Gondwana Research 22, 434–446.

Dan, W., Wang, Q., William, M.W., Zhang, X.Z., Tang, G.J., Jiang, Z.Q., Hao, L.L., Ou, Q., 2018. Rapid formation of eclogites duringa nearly closed ocean: revisiting the Pianshishaneclogite in Qiangtang, central TibetanPlateau. Chemical Geology 477, 112–122.

Day, R., Fuller, M., Schmidt, V.A., 1977. Hysteresis properties of titanomagnetites: grain-size and compositional dependence. Physics of the Earth and Planetary Interiors 13 (4), 260–267.

Dewey, J.F., Shackelton, R.M., Chang, C., Sun, Y., 1988. The tectonic evolution of the Tibetan Plateau. Philosophical Transactions of the Royal Society of London A327, 379–413.

Ding, L., Li, Z.Y., Song, P.P., 2017. Core fragments of Tibetan plateau from Gondwanaland united in northern hemisphere. Progress of comprehensive scientific research on Tibetan plateau, China special issue. Bulletin of Chinese Academy of Sciences 9, 945–950 (in Chinese with English abstract).

Ding, L., Yang, D., Cai, F.L., Pullen, A., Kapp, P., Gehrels, G.E., Zhang, Y.L., Zhang, H.Q., Lai, Z.Q., Yue, H.Y., Shi, R.D., 2013. Provenance analysis of the Mesozoic Hoh-Xil-songpan-Ganziturbidites in northern Tibet: implications for the tectonicevolution of the eastern paleo-Tethys Ocean. Tectonics 32, 34–38.

Domeier, M., Torsvik, T.H., 2014. Plate tectonics in the late Paleozoic. Geoscience Frontiers 5 (3), 303–350.

Dunlop, D.J., 2002. Theory and application of the Day plot (Mrs/Ms versus Hcr/Hc): 1. Theoretical curves and tests using titanomagnetite data. Journal of Geophysical Research 107 (B3), 2056.

Dupont-Nivet, G., van Hinsbergen, D.J.J., Torsvik, T.H., 2010. Persistently low Asian paleolatitudes, implications for the India–Asia collision history. Tectonics 29, 1–19.

Fan, J.J., Li, C., Sun, Z.M., Xu, W., Xie, C.M., 2018. Early Cretaceous MORB-type basalt and A-type rhyolite in northern Tibet: evidence for ridge subduction in the Bangong–Nujiang Tethyan ocean. Journal of Asian Earth Sciences 154 (1), 187–201.

Fan, J.J., Li, C., Xie, C.M., Liu, Y.M., Xu, J.X., Chen, J.W., 2017. Remnants of late Permian-middle Triassic ocean islands in northern Tibet: implications for the late-stage evolution of the paleo-Tethys Ocean. Gondwana Research 44, 7–21.

Fisher, R.A., 1953. Dispersion on a sphere. Proceedings of the Royal Society of London A 217, 295–305.

Fu, G.X., Wang, J., Tan, F.W., 2013. The geological meaning of the late Triassic sedimentary transformation of Qiantang basin in northern Tibet. Geological Review 59, 208–209 (in Chinese).

Fu, X.G., Wang, J., Chen, W.B., Feng, X.L., 2010. Age and tectonic implications of the Late Triassic NadiKangti volcanic rocks in the Qiangtang basin, northern Tibet, China. Journal of Chengdu University of Technology (Science & Technology Edition) 37 (6), 605–615 (in Chinese with English abstract).

Golonka, J., Ford, D., 2000. Pangean (late Carboniferous-middle Jurassic) paleo-environment and lithofacies. Palaeogeography, Palaeoclimatology, Palaeoecology 161, 1–34.

Guo, Z.W., 2013. Composite Stratigraphic Study of the Late Permian – Middle Triassic Strata in the Northern Qiangtang, Mayer Kangri District, Tibet. M.S. thesis. China University of Geosciences, Beijing, p. 57 (in Chinese with English abstract).

Huang, B.C., Chen, J.S., Yi, Z.Y., 2010. Paleomagnetic discussion of when and where India and Asia initially collided. Chinese Journal of Geophysics 53, 2045–2058 (in Chinese with English abstract).

Huang, B.C., Yan, Y.G., Piper, J.D.A., Zhang, D.H., Yi, Z.Y., Yu, S., Zhou, T.H., 2018. Paleomagnetic constraints on the paleogeography of the east Asian blocks during late Paleozoic and early Mesozoic times. Earth-Science Reviews 186, 8–36.

Huang, J.Q., Chen, B.W., 1987. The Evolutional of Tethys in China and Adjacent Regions. Geology Publishing House, Beijing, p. 190 (in Chinese).

Huang, K., Opdyke, N.D., Li, J., Peng, X., 1992a. Paleomagnetism of Cretaceous rocks from eastern Qiangtang terrane of Tibet. Journal of Geophysical Research: Solid Earth 97, 1789–1799.

Huang, K., Opdyke, N.D., Peng, X.J., Li, J.G., 1992b. Paleomagnetic result from the upper Permian of the eastern Qiangtang terrane of Tibet and their tectonic implications. Earth and Planetary Science Letters 111, 1–10.

Huang, S., 2012. Paleomagnetic Investigations on the Cretaceous Volcanic Rocks in South China Block. Ph. D. thesis. Graduate University of Chinese Academy of Sciences, p. 103 (in Chinese with English abstract).

Jackson, M.J., Banerjee, S.K., Marvin, J.A., Lu, R., Gruber, W., 1991. Detrital remanence, inclination errors, and anhysteretic remanence anisotropy, quantitative model and experimental results. Geophysical Journal International 104 (1), 95–103.

King, R.F., 1955. The remanent magnetism of artificially deposited sediment. Geophysical Journal International 7 (s3), 115–134.

Kirschvink, J.L., 1980. The least–square line and plane and the analysis of paleomagnetic data. Geophysical Journal of the Royal Astronomical Society 62, 699–718.

Kodama, K.P., Sun, W.W., 1992. Magnetic anisotropy as a correction for compaction-caused palaeomagnetic inclination shallowing. Geophysical Journal International 111 (3), 465–469.

Lei, Z.Y., Li, Y.T., Liu, Z., Lu, B., 2001. Structural deformation and dynamic mechanism of the Qiangtang basin, north Tibet. Geological Review 47 (4), 415–419.

Li, C., Zhai, G.Y., Wang, L.Q., Yin, F.G., Mao, X.C., 2009. An important window for understanding the Qinghai – Tibet Plateau – a review on research progress in recent years of Qiangtang area, Tibet, China. Geological Bulletin of China 28 (9), 1169–1177 (in Chinese with English abstract).

Li, C., Zheng, A., 1993. Paleozoic stratigraphy in the Qiangtang region of Tibet: relations of the Gondwana and Yangtze continents and ocean closure near the end of the Carboniferous. International Geological Reviews 35 (9), 797–804.

Li, S.P., Wang, Y.Z., Shen, C.X., Xu, C.Q., Qi, S.S., Zeng, X.P., 2007. Geochemical characteristics of the late Permian-early Triassic continental volcanic rocks in the Zadoi area, northern Qiantang, Tibet plateau. Geological Bulletin of China 26 (6), 675–681 (in Chinese with English abstract).

Li, Y.L., Wang, C.S., Huang, J.J., 2008. Deformation characteristics and finalizing age of the folds in the Qiangtang Basin angle their relations to oil and gas accumulation. Oil & Gas Geology 29 (3), 283–290 (in Chinese with English abstract).

Li, Y.L., Wang, C.S., Zhao, X.X., Yin, A., Ma, C., 2012. Cenozoic thrust system, basin evolution, and uplift of the Tanggula Range in the Tuotuohe region, central Tibet. Gondwana Research 22, 482–492.

Li, J.T., Liang, B., He, W.J., Xu, G., Weng, L., Xie, Q.X., 2016a. Geological and tectonic evolution of the basement in the Qiangtang basin of northern Tibet: evidence from detrital zircon U-Pb isotope chronology of sandstone in the Jurassic Yanshipin Group. Geology in China 43 (4), 216–1226 (in Chinese with English abstract).

Li, Z.Y., Ding, L., Lippert, P.C., Song, P.P., Yue, Y.H., van Hinsbergen, D.J.J., 2016b. Paleomagnetic constraints on the Mesozoic drift of the Lhasa terrane (Tibet) from Gondwana to Eurasia. Geology 44, 727–730.

Li, Z.Y., Ding, L., Song, P.P., Fu, J.J., Yue, Y.H., 2017. Paleomagnetic constraints on the paleolatitude of the Lhasa block during the Early Cretaceous: implications for the onset of India–Asia collision and latitudinal shortening estimates across Tibet and stable Asia. Gondwana Research 41, 352–372.

Liebke, U., Appel, E., Ding, L., Neumann, U., Antolin, B., Xu, Q., 2010. Position of the Lhasa terrane prior to India–Asia collision derived from palaeomagnetic inclinations of 53 Ma old dykes of the Linzhou Basin: constraints on the age of collision and postcollisional shortening within the Tibetan Plateau. Geophysical Journal International 182, 1199–1215.

Lin, J., Watts, D.R., 1988. Palaeomagnetic results from the Tibetan plateau. Philosophical Transactions of the Royal Society of London,Series A 327, 239–262.

Lippert, P.C., Dupont-Nivet, G., van Hinsbergen, D.J.J., Zhao, X., Coe, R.S., Kapp, P., 2010. The Paleogene latitude of Asia and the proto-Tibetan plateau. Open-File Report 2010-1099. In: Leech, M.L., others (Eds.), Proceedings for the 25th Himalaya-Karakoram-Tibet Workshop. U.S. Geological Survey, 2pp.

Liu, Y., Sun, K.Q., 2008. Study on the Permian paleophytogeographical provinces in Xizang (Tibet). Geological Review 54 (3), 289–295 (in Chinese with English abstract).

Liu, Y., Li, R.S., Ji, W.H., Pan, S.J., Chen, F.N., Zhang, H.D., 2014. The pairing relationship between ophiolite and arc volcanic rocks along western Jinsha River suture zone and its geological significance: evidence from geochemistry and LA-ICP-MS zircon U-Pb dating. Geological Bulletin of China 33 (7), 1076–1088 (in Chinese with English abstract).

Lowrie, W., 1990. Identification of ferromagnetic minerals in a rock by coercivity and unblocking temperature properties. Geophysical Research Letters 17, 159–162.

Ma, Y.M., Wang, Q., Wang, J., Yang, T.S., Tan, X.D., Wei, Dan, Zhang, X.Z., Ma, L., Wang, Z.L., Hu, W.L., Zhang, S.H., Wu, H.C., Li, H.Y., Cao, L.W., 2019. Paleomagnetic constraints on the origin and drift history of the north Qiangtang terrane in the late Paleozoic. Geophysical Research Letters 46, 689–697.

McElhinny, M., 1964. Statistical significance of the fold test in paleomagnetism. Geophysical Journal International 8, 338–340.

McFadden, P., 1990. A new fold test for palaeomagnetic studies. Geophysical Journal International 103, 163–169.

Metcalfe, I., 1996. Gondwanaland and dispersion, Asian accretion and evolution of eastern Tethys. Australian Journal of Earth Sciences 43, 605–623.

Metcalfe, I., 2013. Gondwana dispersion and Asian accretion: tectonic and palaeogeographic evolution of eastern Tethys. Journal of Asian Earth Sciences 66, 1–33.

Otofuji, Y., Inoue, Y., Funahara, S., Murata, F., Zheng, X., 1990. Palaeomagnetic study of eastern Tibet-deformation of the three rivers region. Geophysical Journal International 103, 85–94.

Pan, G.T., Wang, L.Q., Li, R.S., Yuan, S.H., Ji, W.H., Yin, F.G., Zhang, W.P., Wang, B.D., 2012. Tectonic evolution of the Qinghai–Tibet plateau. Journal of Asian Earth Sciences 53, 3–14.

Pearce, J.A., Mei, H., 1988. Volcanic rocks of the 1985 Tibet Geotraverse: Lhasa to Golmud. Philosophical Transactions of the Royal Society, Mathematical, Physical Engineer Science 327, 169–201.

Pullen, A., Kapp, P., 2014. Mesozoic tectonic history and lithospheric structure of the Qiangtang terrane: insights from the Qiangtang metamorphic belt, central Tibet. Geological Society of London Specical Publications and remove dot 507, 71–87.

Qinghai BGMR, Qinghai Bureau of Geology and Mineral Resources, 2005. 1:250,000 Regional Geology of the Tuotuohe Region. Geological Publishing House, Beijing (in Chinese).

Qu, L.H., Liu, X.F., Li, J.S., Qi, L.J., 2015. Geochemical characteristics of sedimentary rocks from the Triassic Kanglu Formation, north Qiangtang basin (Tibet): implications for provenance tectonic setting. Geoscience 29 (4), 789–803 (in Chinese with English abstract).

Ran, B., Deng, B., Wang, C.S., Zhao, X.X., Li, Y.L., Zhang, Y.X., Meng, J., He, M., Zhu, L.D., Xiao, C., 2017. Kinematics of the crust around the Tanggula Shan in north–central Tibet: constraints from paleomagnetic data. Gondwana Research 48, 124–133.

Ran, B., Wang, C.S., Zhao, X.X., Li, Y.L., He, M., Zhu, L.D., Coe, R.S., 2012. New paleomagnetic results of the early Permian in the Xainza area, Tibetan Plateau and their paleogeographical implications. Gondwana Research 22, 447–460.

Ren, J.S., Xiao, L.W., 2004. Lifting the mysterious veil of the tectonics of the Qinghai–Tibet Plateau by 1:250000 geological mapping. Geological Bulletin 23 (1), 1–11 (in Chinese with English abstract).

Song, C.Y., Wang, J., Fu, X.G., Feng, X.L., Chen, M., He, L., 2012. Late Triassic palaeomagnetic data from the Qiangtang terrane of Tibet plateau and their tectonic significances. Journal of Jilin University (Earth Science Edition) 42 (2), 526–535 (in Chinese with English abstract).

Song, P.P., Ding, L., Li, Z.Y., Lippert, P.C., Yang, T., Zhao, X., Fu, J., Yue, Y., 2015. Late Triassic paleolatitude of the Qiangtang block: implications for the closure of the paleo-Tethys Ocean. Earth and Planetary Science Letters 424, 69–83.

Song, P.P., Ding, L., Li, Z.Y., Lippert, P.C., Yue, Y.H., 2017. An early bird from Gondwana: paleomagnetism of lower Permian lavas from northern Qiangtang (Tibet) and the geography of the paleo-Tethys. Earth and Planetary Science Letters 475, 119–133.

Sun, Z.M., Cao, Y., Li, H.B., Pei, J.L., Tong, Y.B., Ye, X.Z., Wu, B.L., Cao, X.W., Liu, C.G., 2019. A review of paleomagnetic study of the formation and evolution of the Tibetan plateau. Acta Geoscientica Sinica 40 (1), 17–36 (in Chinese with English abstract).

Tang, C.Y., Wu, J.H., Wang, G.Q., Zhao, W.Q., Wang, J.X., 2011. Sedimentary evolution of the upper Triassic Jiapila Formation at the Middle Qiangtang basin and its geological significance. Geotectonica et Metallogenia 35 (3), 421–428 (in Chinese with English abstract).

Tapponnier, P., Xu, Z.Q., Roger, F., Meyer, B., Arnaud, N., Wittlinger, G., Yang, J.S., 2001. Oblique stepwise rise and growth of the Tibet plateau. Science 294, 1671–1677.

Tauxe, L., Kent, D.V., 2004. A simplified statistical model for the geomagnetic field and the detection of shallow bias in paleomagnetic inclinations: was the ancient magnetic field dipolar? In: Channell, J.E.T., Kent, D.V., Lowrie, W., Meert, J.M. (Eds.), Timescales of the Paleomagnetic Field: AGU Geophysical Monograph Series, vol. 145, pp. 101–115.

Tong, Y.B., Yang, Z.Y., Gao, L., Wang, H., Zhang, X.D., An, C.Z., Xu, Y.C., Han, Z.R., 2015. Paleomagnetism of upper Cretaceous red-beds from the eastern Qiangtang block: clockwise rotations and latitudinal translation during the India–Asia collision. Journal of Asian Earth Sciences 114, 732–749.

Torsvik, T.H., Van der Voo, R., Preeden, U., Mac Niocaill, C., Steinberger, B., Doubrovine, P.V., van Hinsbergen, D.J.J., Domeier, M., Gaina, C., Tohver, E., Meert, J.G., McCausland, P.J.A., Cocks, L.R.M., 2012. Phanerozoic polar wander, palaeo-geography and dynamics. Earth-Science Reviews 114, 325–368.

Van der Voo, 1990. The reliability of paleomagnetic data. Tectonophysics 184, 1–9.

Wang, C.S., Zheng, H.R., Ran, B., Liu, B.P., Li, X.H., Li, Y.L., Sun, H.J., Chen, J.P., Hu, X.M., 2010. On paleogeographic reconstruction, an example for application in Tibetan Tethys. Acta Sedmentologica Sinica 28 (5), 849–859 (in Chinese with English abstract).

Wang, G.Z., Wang, C.S., 2001. Disintegration and age of basement metamorphic rocks in Qiangtang, Tibet, China. Science China Earth Sciences 44, 86–93.

Wang, J., Fu, X.G., 2018. Sedimentary evolution of the Qiangtang basin. Geology in China 45 (2), 237–259 (in Chinese with English abstract).

Wang, N.W., 1984. The rise of Gondwana research in China and some key problems on paleobiogeography related to plate tectonics. Bulletin of the Chinese Academy of Geological Sciences 10, 104–114 (in Chinese).

Watson, G.S., Enkin, R.J., 1993. The fold test in paleomagnetism as a parameter estimation problem. Geophysical Research Letters 20, 2135–2137.

Weislogel, A.L., 2008. Tectonostratigraphic and geochronologic constraint son evolution of the northeast Paleotethys from the Songpan - Ganzi complex, central China. Tectonophysics 451 (1–4), 331–345.

Wu, F.Y., Huang, B.C., Ye, K., Fang, A.M., 2008. Collapsed Himalayan-Tibetan orogeny and the rising Tibetan plateau. Acta Petrologica Sinica 24 (1), 1–30 (in Chinese with English abstract).
Wu, L., Kravchinsky, V.A., Potter, D.K., 2017a. Apparent polar wander paths of the major Chinese blocks since the Late Paleozoic: toward restoring the amalgamation history of east Eurasia. Earth-Science Reviews 17, 492–519.
Wu, Y.W., Li, C., Xu, M.J., Xie, C.M., Wang, M., 2017b. Zircon U-Pb age, geochemical data: constraints on the origin and tectonic evolution of the metamafic rocks from Longmuco-Shuanghu-Lancang suture zone, Tibet. Journal of Earth Sciences 28 (3), 422–432.
Xiao, W.J., Ao, S.J., Yang, L., Han, C.M., Wan, B., Zhang, J.E., Zhang, Z.Y., Li, R., Chen, Z.Y., Song, S.H., 2017. Anatomy of composition and nature of plate convergence: insights for alternative thoughts for terminal India-Eurasia collision. Science China Earth Sciences 60, 1015–1039.
Xiao, W.J., Windley, B., Sun, S., Li, J.L., Huang, B.C., Han, C.M., Chao, Y., Sun, M., Chen, H.L., 2015. A tale of amalgamation of three Permo-Triassic collage systems in Central Asia: oroclines, sutures, and terminal accretion. Annual Review of Earth and Planetary Sciences 16, 1–16.31.
Xie, C.M., Li, C., Ren, Y.S., Wang, M., Su, L., 2018. Detrital provenance, depositional environment, and palaeogeographic implications of Lower Triassic marine sediments in central Tibet. International Geology Review 60 (4), 418–430.
Xu, Y.C., Yang, Z.Y., Tong, Y.B., Wang, H., Gao, L., An, C.Z., 2015. Further paleomagnetic results for lower Permian basalts of the Baoshan Terrane, southwestern China, and paleogeographic implications. Journal of Asian Earth Sciences 104, 99–114.
Yan, M., Zhang, D., Fang, X., Ren, H., Zhang, W., Zan, J., Song, C., Zhang, T., 2016. Paleomagnetic data bearing on the Mesozoic deformation of the Qiangtang block: implications for the evolution of the paleo- and meso-Tethys. Gondwana Research 39, 292–316.
Yan, Y.G., Huang, B.C., Zhang, D.H., Veeravinantanakul, A., 2018. Paleomagnetic study on the Permian rocks of the Indochina Block and its implications for paleogeographic Configuration and northward drifting of Cathaysialand in the paleo-Tethys. Journal of Geophysical Research 128 (6), 4523–4538.
Yang, T.S., Ma, Y.M., Zhang, S.H., Bian, W.W., Yang, Z.Y., Wu, H.C., Li, H.Y., Chen, W.W., Ding, J.K., 2015. New insights into the India–Asia collision process from Cretaceous paleomagnetic and geochronologic results in the Lhasa terrane. Gondwana Research 28, 625–641.
Yang, X.F., Cheng, X., Zhou, Y.N., Lun, M.A., Zhang, X.D., 2017. Paleomagnetic results from Late Carboniferous to Early Permian rocks in the northern Qiangtang terrane, Tibet, China, and their tectonic implications. Science China Earth Sciences 60 (1), 124–134.
Ye, X.H., Li, J.F., 1987. Paleomagnetism and evolution of Tibet plates and Tethys. Journal of Chengdu College of Geology 14 (1), 65–79 (in Chinese with English abstract).
Yi, Z.Y., Liang, Y.L., Zhao, J., Yan, Y.Y., Chen, L.W., Tan, X.D., 2016. Paleogeography of the northern margin of Indian continent prior to its collision: an investigation of the late Cretaceous limestone in south Tibet. Acta Geologica Sinica 90 (11), 3282–3292 (in Chinese with English abstract).
Yin, A., Harrison, T.M., 2000. Geologic evolution of the Himalayan-Tibetan orogen. Annual Review of Earth and Planetary Sciences 28, 211–280.
Zeng, X.W., Wang, M., Fan, J.J., Cai, L., Xie, C.M., Liu, Y.M., Zhang, T.Y., 2018. Geochemistry and geochronology of gabbros from the asa ophiolite, Tibet: implications for the early Cretaceous evolution of the Meso-Tethys Ocean. Lithos 320–321, 192–206.
Zhang, D., Huang, B., Zhao, J., Meert, J.G., Zhang, Y., Liang, Y., Bai, Q., Zhou, T., 2018. Permian paleogeography of the eastern CAOB: paleomagnetic constraints from volcanic rocks in central eastern Inner Mongolia, NE China. Journal of Geophysical Research: Solid Earth 123 (4), 2559–2582.
Zhang, J., 2017. Combined Paleomagnetic and Geochronological Study on the Late Permian Strata of the Qiangbei-Changdu Block. M.S. thesis. Northwest University, p. 68. pp (in Chinese with English abstract).
Zhang, K.J., Tang, X.C., 2009. Eclogites in the interior of the Tibetan plateau and their geodynamic implications. Chinese Science Bulletin 54, 2556–2567.
Zhang, K.J., Zhang, Y.X., Li, B., Zhu, Y.T., Wei, R.Z., 2006. The blueschist-bearing Qiangtang metamorphic belt (northern Tibet, China) as an in situ suture zone: evidence from geochemical comparison with the Jinsa suture. Geology 34, 493–496.
Zhang, P.Z., Wang, Q., Ma, Z.J., 2002. GPS velocity field and active crustal blocks of contemporary tectonic deformation in continental China. Earth Science Frontiers 9 (2), 430–441 (in Chinese with English abstract).
Zhang, Y.C., Shi, G.R., Shen, S.Z., 2013. A review of Permian stratigraphy, palaeobiogeography and paleogeography of the Qinghai–Tibet Plateau. Gondwana Research 24, 55–76.
Zhao, J., Huang, B.C., Yan, Y.G., Zhang, D.H., 2015. Late Triassic paleomagnetic result from the Baoshan terrane, West Yunnan of China: implication for orientation of the east Paleotethyssuture zone and timing of the sibumasu-indochina collision. Journal of Asian Earth Sciences 111, 350–364.
Zheng, Y.L., Wang, G.H., Guo, Z.W., Liang, X., Yuan, G.L., Wang, H.D., Huang, B., He, Y.D., 2015. The record of the Pan-African and the Indosinian tectonothermal event in Qiangtang terrane, northern Tibet: evidence from geochemical characteristics and U-Pb geochronology of the metamorphic complex in Ejiumai area. Acta Petrologica Sinica 31 (4), 1137–1152 (in Chinese with English abstract).
Zhong, D.L., Ding, L., 1996. The process and mechanism of the uplift of the Tibetan Plateau China. Science China Earth Sciences 26 (4), 289–295 (in Chinese).
Zhou, Y., Cheng, X., Yu, L., Yang, X.F., Su, H.L., Peng, X.M., Xue, Y.K., Li, Y.Y., Ye, Y.K., Zhang, J., Li, Y.Y., Wu, H.N., 2016. Paleomagnetic study on the Triassic rocks from the Lhasa terrane, Tibet, and its paleogeographic implications. Journal of Asian Earth Sciences 121, 108–119.
Zhu, D., Li, S., Cawood, P.A., Wang, Q., Zhao, Z., Liu, S., Wang, L., 2016. Assembly of the Lhasa and Qiangtang terranes in central Tibet by divergent double subduction. Lithos 245, 7–17.
Zhu, T.X., Feng, X.T., Wang, X.F., Zhou, M.K., 2010. Late Triassic tectonic-paleogeography of the Qiangtang area on the Qinghai-Xizang plateau. Sedimentary Geology and Tethyan 30 (4), 1–10 (in Chinese with English abstract).
Zhu, T.X., Li, Z.L., Li, C., Feng, X.T., Zhang, Q.Y., Zhang, H.H., Lin, S.L., Zeng, Q.R., 2005. New data of Triassic strata in the Shuanghu area, northern Tibet, China. Geological Bulletin of China 25 (12), 1127–1134 (in Chinese with English abstract).
Zijderveld, J.D.A., 1967. A. C. demagnetization of rocks: analysis of results. In: Collinson, D.W., Creer, K.M., Runcorn, S.K. (Eds.), Methods on Paleomagnetism. Elsevier, Amsterdam, pp. 254–286.